AD-A093 037 NATIONAL AERONAUTICAL ESTABLISHMENT OTTAWA (ONTARIO) F/G 1/3
A METHOD FOR THE PREDICTION OF WING RESPONSE TO NON-STATIONARY --ETC(U)
JUL 80 B H LEE
UNCLASSIFIED NAE-LR-601 NRC-18629 NL

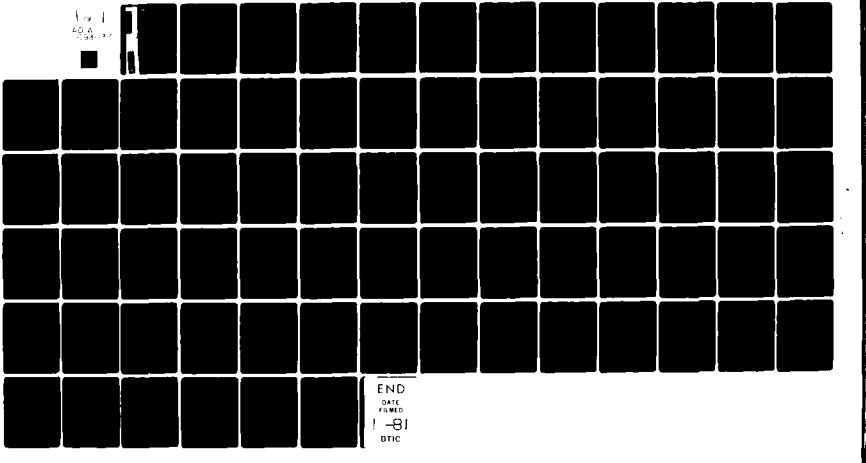

END
DATE FILMED
1-81
DTIC

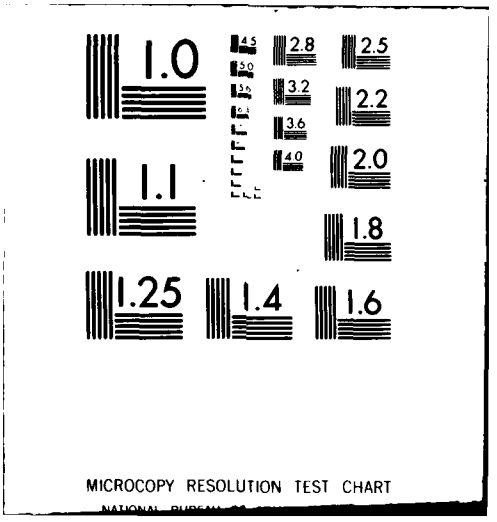
1.0
1.1
1.25
1.4
1.6
1.8
2.0
2.2
2.5
2.8
3.2
3.6
4.0
4.5
MICROCOPY RESOLUTION TEST CHART

National Research Council Canada
Conseil national de recherches Canada

A METHOD FOR THE PREDICTION OF WING RESPONSE TO NON-STATIONARY BUFFET LOADS

by

B.H.K. Lee

National Aeronautical Establishment

OTTAWA
JULY 1980

NRC NO. 18629

AERONAUTICAL REPORT LR-601

A METHOD FOR THE PREDICTION OF WING RESPONSE TO NON-STATIONARY BUFFET LOADS

MÉTHODE DE PRÉVISION DE LA RÉPONSE D'UNE AILE SOUS DES CHARGES DE BUFFETING INSTATIONNAIRES

by/par

B.H.K. Lee

L.H. Ohman, Head/Chef
High Speed Aerodynamics Laboratory/
Laboratoire d'aérodynamique à hautes vitesses

G.M. Lindberg
Director/Directeur

SUMMARY

A method for the prediction of the response of a wing to non-stationary buffet loads is presented. The time history of the applied load is segmented into a number of time intervals. In each time segment, the non-stationary load is represented by the product of a deterministic shaping function and a statistically stationary random function. An approximate modelling of the load on the wing is given. The wing is divided into panels or elements, and the load is computed from measured or estimated pressure fluctuations at the centre of each panel. A series representation, with terms of the correlated noise type, is used to curve fit the experimentally determined complex buffet pressure power spectral densities. Using the correlated noise form of power spectral density for the random part of the applied load, analytic expressions are derived for the mean square displacement and acceleration response of the wing. An illustration using data available for the F-4E aircraft is included.

RÉSUMÉ

La présente communication porte sur une méthode de prévision du comportement d'une aile sous des charges de buffeting instationnaires. L'évolution de la charge appliquée est divisée en intervalles de temps. Dans chaque intervalle, la charge non fixe est représentée par le produit d'une fonction de "forme" déterministe et d'une fonction aléatoire statistiquement stationnaire. Un modèle approché de la charge sur l'aile est donné. L'aile est divisée en panneaux ou éléments, et la charge est calculée à partir des fluctuations de pression mesurées ou estimées au centre de chaque panneau. Un développement en série, comportant des termes du type bruit correlé, sert à ajuster à une courbe les densités spectrales complexes de pression de buffeting qui sont déterminées expérimentalement. Des expressions analytiques du carré moyen de la réponse de l'aile en déplacement et en accelération sont dérivées de la fonction de type bruit correlé de la densité spectrale pour la composante aléatoire de la charge appliquée. Un exemple s'appuyant sur les données existantes sur l'avion F-4E est donné.

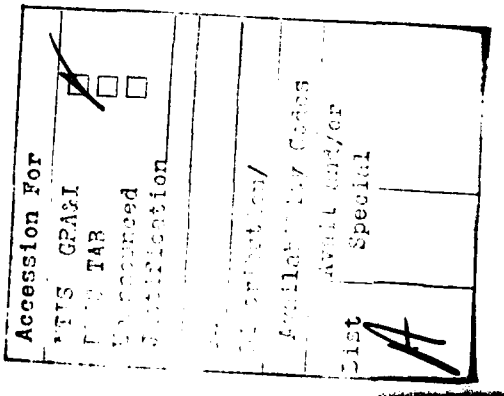

CONTENTS

ILLUSTRATIONS

ILLUSTRATIONS (Cont'd)

APPENDICES

SYMBOLS

Symbols	Definition
A	area of a panel
b	wing semi-span
C	generalized damping coefficient
$\Delta C_{p_{rms}}$	root mean square fluctuating pressure divided by free stream dynamic pressure
$E[z^2(t)]$	expected value of z(t)
$\tilde{E}[\ ]$	expected value defined in Equation (37)
$\tilde{E}^{km}[\ ]$	expected value defined in Equation (40)
$\bar{E}[\ ]$	non-dimensional expected value defined in Equations (60) and (67)
$\bar{E}^{k}[\ ]$	non-dimensional expected value at the centre of a panel defined in Equation (73)
f(t)	stationary force
$H(\omega)$	frequency response function
$I(t,\omega)$	time dependent frequency response function
I	number of modes
K	generalized stiffness; also number of panels
L(t)	generalized force
M	generalized mass; also number of terms used in series expression for power spectral density

SYMBOLS (Cont'd)

Symbols	Definition
p_{rms}	root mean square value of fluctuating pressure
q	dynamic pressure
r	distance between centres of two panels
$R_{L_iL_j}(t_1,t_2)$	correlation between $L_i(t_1)$ and $L_j(t_2)$
$S_{L_iL_j}(\omega_1,\omega_2)$	power spectral density of applied load given in Equation (14)
$S_p(\omega)$	pressure power spectral density
t,T	time
T_B	duration aircraft spent in buffet régime or duration of applied load
Δt_r	duration of time segment
$u(t)$	*unit step function*
V	aircraft velocity
x,y	co-ordinate system defined in Figure 4
$\bar{y}$	distance measured from wing root along a constant percentage chord line
z	displacement
α_r^{km}	constant in Equation (38)
β_r^{km}	constant in Equation (38)
$\beta_r(t)$	$u(t-t_{r-1}) - u(t-t_r)$
$\gamma(t)$	deterministic function
δ	spatial decay coefficient; also displacement amplitude decrement in percentage
ϵ	intensity of applied load
ζ	damping ratio
ρ	density; also designate poles in the complex plane
τ	delay, t_1-t_2

SYMBOLS (Cont'd)

Symbols	Definition
ϕ	mode shape function
ω	frequency
ω_d	damped natural frequency
ω_n	undamped natural frequency
Subscripts:	
'L'	denotes applied load
'r', 's', 'q'	denote the rth, sth or qth time segment
'i', 'j'	denote the ith or jth vibration mode
'k', 'ℓ'	denote the kth or ℓth panel
Superscripts:	
'k'	denotes the kth panel
'm'	denotes the mth term in the series expression for the power spectral density
'′'	denotes non-dimensional time with respect to the undamped natural period T_1 of the first vibration mode
'—'	denotes non-dimensional quantities
'•'	differentiation with respect to time
'••'	denotes second derivative with respect to time

A METHOD FOR THE PREDICTION OF WING RESPONSE TO NON-STATIONARY BUFFET LOADS

1.0 INTRODUCTION

Buffeting is the aeroelastic response of aircraft structures to aerodynamic excitation arising from random loading due to flow separations on the wing. It is almost always encountered when the aircraft approaches the limiting useable lift at high speeds. The maneuvering capability of aircrafts in the transonic speed range is thus usually limited by buffet or buffet-related unsteady phenomena which induce the pilot to restrict the maneuver. Methods for predicting the buffet intensity as the aircraft penetrates into the buffet régime are extremely useful and much needed in aircraft design.

The random nature of the loading on the wing due to flow separations requires statistical theory in predicting the dynamic response of the wing during buffeting. Considering the exciting force to be statistically stationary, Liepman (Ref. 1) examined the problem of the lift force exerted on a two-dimensional thin airfoil moving in turbulent air. Later, he extended the method to wings of finite span (Ref. 2). The analysis was generalized by Ribner (Ref. 3) using a model of turbulence represented by the superposition of plane sinusoidal shear waves of all orientations and wavelengths. The correlations between flight and wind tunnel tests with predictions based on statistical approach had been reported by various investigators (e.g., Refs. 4-8). Amongst the more recent studies on this subject are those of Mullans and Lemley (Ref. 9), Hwang and Pi (Refs. 10, 11). Cunningham et al. (Ref. 12), Jones (Ref. 13), and Butler and Spavins (Ref. 14). Because of the complexities of the buffet phenomenon, the above methods incorporate numerous simplifying assumptions and hence, can only be considered to be approximate. However, they are invaluable in providing buffet information during the early stages of aircraft design.

The assumption of statistical stationarity used in the above prediction methods can be justified as long as the flight conditions are unchanged within a reasonably long analysis time when measurements are made of either the buffet load or the wing response. In wind tunnel testing, statistical stationarity requires long running time compared to the natural period of the mode of vibration under investigation. When these conditions are not met, such as in rapid maneuvers or in short duration wind tunnel testing, a non-stationary analysis of the wing response has to be considered.

An approximate solution of the transient response of a wing to a buffet load having a parabolic variation of its rms value with time was given by Zbrozek and Jones (Ref. 15). In Reference 16, a method for estimating the response of a wing to non-stationary buffet loads was developed and applied to a number of examples involving different aircraft maneuvers. The analysis was based on a theory of the non-stationary response of linear dynamic systems first given by Caughey and Stumpf (Ref. 17), and later extended by Barnoski and Maurer (Ref. 18), and Holman and Hart (Ref. 19). Various forms of the power spectral density for the random part of the input load were investigated, and expressions were derived for the mean square response of the wing displacement. In Reference 20, it was shown that if the loading on the wing was to compose of fluctuating forces from various uncorrelated sources, a series representation could be used to represent fairly complex buffet load spectra. The total response could be obtained from a summation of the individual responses to each term in the series. The analysis was further extended in Reference 21 to include multi-modal response of a wing to non-stationary buffet loads for those cases when the undamped natural frequencies of individual modes were close together and the modes of vibration were statistically dependent.

This report describes a method for predicting the mean square displacement and acceleration response of a wing to non-stationary buffet loads by extending the analyses of References 16, 20 and 21. The time history of the applied load is segmented into a number of time intervals. In each time segment, the non-stationary load is represented by the product of a deterministic shaping function and a statistically stationary random function. The total response to a given maneuver is obtained by summation of the responses of the wing from each time segment. Unlike the approach used in References 16, 20 and 21, which assume a known integrated buffet load over the wing, the present study gives an

approximate modelling of the load on the wing. This is based on a modification of a method proposed by Schweiker and Davies (Ref. 22) for the study of the response of shells to aerodynamic noise. In essence, the method divides the wing into panels or elements, and the load is computed from measured or estimated pressure fluctuations at the centre of each panel. Following the approach used in Reference 20, a series representation, with terms of the correlated noise type, is used to represent the complex buffet pressure power spectral densities. Some computed response results are presented for the F-4E wing as an example, using experimental fluctuating pressure data obtained by Mullans and Lemley (Ref. 9).

2.0 ANALYSIS

2.1 Dynamic Aeroelastic Equations

Consider a Cartesian co-ordinate system x, y and z fixed on the wing as illustrated in Figure 1. The displacement of the wing can be expressed in terms of a set of normal co-ordinates $z_i(t)$ as:

$$z(x,y,t) = \sum_{i=1}^{I} \phi_i(x,y) z_i(t) \tag{1}$$

where $\phi_i(x,y)$ is the mode shape function of the ith mode, and I is the number of modes required to adequately represent z(x,y,t) in the form of a series. The dynamic aeroelastic equations governing the response of $z_i(t)$ to an input load $L_i(t)$ is given in generalized co-ordinates as:

$$M_i \ddot{z}_i + C_i \dot{z}_i + K_i z_i = L_i(t) \tag{2}$$

for the ith mode. The dots denote differentiation with respect to time, M_i, C_i and K_i are the generalized mass, damping coefficient and stiffness of the ith mode respectively. In the above equation, the assumption of light damping is made, thus, cross damping terms do not appear.

Define the undamped natural frequency ω_{i_n} as:

$$\omega_{i_n}^2 = \frac{K_i}{M_i} \tag{3}$$

and the damping ratio ζ_i as:

$$\zeta_i = \frac{C_i}{2\sqrt{M_i K_i}} \tag{4}$$

Using the above two expressions, Equation (2) can be rewritten as follows:

$$\ddot{z}_i + 2\zeta_i \omega_{i_n} \dot{z}_i + \omega_{i_n}^2 z_i = \frac{1}{M_i} L_i(t) \tag{5}$$

The generalized force can be expressed in terms of the fluctuating pressure p(x,y,t) as:

$$L_i(t) = \iint_{\substack{\text{wing} \\ \text{planform}}} \phi_i(x,y) p(x,y,t) dx dy \tag{6}$$

where the integration is taken over the wing surface.

2.2 Response to Non-Stationary Input

From Equation (1), the mean square response of the displacement of the wing can be written in the following form:

$$E[z^2(x,y,t)] = \sum_{i=1}^{I} \sum_{j=1}^{I} \phi_i(x,y)\phi_j(x,y)E[z_i(t)z_j(t)] \tag{7}$$

For i = j, $\phi_i^2(x,y)E[z_i^2(t)]$ gives the mean square response of the ith mode at the point (x,y) on the wing. If $i \neq j$, $\phi_i(x,y)\phi_j(x,y)E[z_i(t)z_j(t)]$ is the contribution to the total response due to correlation between the ith and jth modes.

For a given buffet maneuver, the mean square loading on the wing versus time may be represented schematically as in Figure 2. The points A and B correspond to the onset and exit of buffeting respectively. The time duration the aircraft spends in the buffet regime is denoted by T_B. The load is non-stationary and time varying properties, such as the mean square of the response, can only be determined by instantaneous averaging over an ensemble. The time segmentation technique used in References 16, 20 and 21 divides the time T_B into a number of intervals or segments. Within each segment, the load is represented by the product of a deterministic time function and a stationary random function. The random function may not necessarily be the same in each segment. Using the subscript 'r' to denote the rth segment, the generalized force for the ith mode at time t can be written as:

$$L_i(t) = \sum_{r=1}^{n} \gamma_r(t) f_{i_r}(t) \tag{8}$$

where $f_{i_r}(t)$ is a stationary random function, and $\gamma_r(t)$ is a deterministic function of time which may be considered as a shaping function written in the following form:

$$\gamma_r(t) = \epsilon_r \beta_r(t) \tag{9}$$

where

$$\beta_r(t) = u(t-t_{r-1}) - u(t-t_r) \tag{10}$$

Here u(t) is a unit step function, ϵ_r is a constant at each time segment and represents the intensity of the generalized input load. Figure 3 illustrates the variation of ϵ with time and shows an approximate description of a continuously varying load using the time segmentation method. However, such a representation can be exact in practice, for example, in wind tunnel testing where the model angle of incidence advances in steps with time in a prescribed manner so that the buffet load can be represented by Equation (8) without any approximation.

Introduce a frequency response function $H_i(\omega)$ as

$$H_i(\omega) = \frac{1}{M_i\left[\omega_{i_n}^2 - \omega^2 + i2\zeta_i\omega\omega_{i_n}\right]} \tag{11}$$

The correlation between $L_i(t_1)$ and $L_j(t_2)$ can be written as:

$$R_{L_iL_j}(t_1,t_2) = \sum_{r=1}^{n} \sum_{s=1}^{n} \gamma_r(t_1)\gamma_s(t_2)R_{f_{i_r}f_{j_s}}(t_1,t_2) \tag{12}$$

Since $f_{i_r}(t_1)$ and $f_{j_s}(t_2)$ are assumed to be stationary, then

$$R_{f_{i_r}f_{j_s}}(t_1,t_2) = R_{f_{i_r}f_{j_s}}(\tau) = \int_{-\infty}^{\infty} S_{f_{i_r}f_{j_s}}(\omega)e^{i\omega\tau}d\omega \tag{13}$$

where $\tau = t_1 - t_2$. Using Equations (12) and (13) and the generalized Wiener-Khinchine relation (Ref. 23), $S_{L_iL_j}(\omega_1,\omega_2)$ can be expressed as

$$S_{L_iL_j}(\omega_1,\omega_2) = \sum_{r=1}^{n}\sum_{s=1}^{n}\int_{-\infty}^{\infty} S_{f_{i_r}f_{j_s}}(\omega)A_{i_r}(\omega-\omega_1)A_{j_s}^*(\omega-\omega_2)d\omega \tag{14}$$

where
$$A_{i_r}(\omega-\omega_1) = \frac{1}{2\pi}\int_{-\infty}^{\infty}\gamma_r(t_1)e^{i(\omega-\omega_1)t_1}dt_1 \tag{15}$$

and
$$A_{j_s}^*(\omega-\omega_2) = \frac{1}{2\pi}\int_{-\infty}^{\infty}\gamma_s(t_2)e^{-i(\omega-\omega_2)t_2}dt_2 \tag{16}$$

The correlation of $z_i(t_1)$ and $z_j(t_2)$ can be expressed in terms of the power spectral density of the applied load $S_{L_iL_j}(\omega_1,\omega_2)$ as follows:

$$R_{z_iz_j}(t_1,t_2) = \int_{-\infty}^{\infty}\int_{-\infty}^{\infty} S_{L_iL_j}(\omega_1,\omega_2)H_i(\omega_1)H_j^*(\omega_2)e^{i(\omega_1t_1-\omega_2t_2)}d\omega_1\,d\omega_2 \tag{17}$$

where $H_i(\omega_1)$ is given by Equation (11) and $H_j^*(\omega_2)$ is the complex conjugate of $H_j(\omega_2)$. Substituting Equation (14) into the above equation results in the following:

$$R_{z_iz_j}(t_1,t_2) = \sum_{r=1}^{n}\sum_{s=1}^{n}\int_{-\infty}^{\infty} S_{f_{i_r}f_{j_s}}(\omega)I_{i_r}(t_1,\omega)I_{j_s}^*(t_2,\omega)d\omega \tag{18}$$

where $I(t,\omega)$ is the time dependent frequency response function defined as:

$$I_{i_r}(t_1,\omega) = \int_{-\infty}^{\infty} A_{i_r}(\omega-\omega_1)H_i(\omega_1)e^{i\omega_1t_1}d\omega_1 \tag{19}$$

and
$$I_{j_s}^*(t_2,\omega) = \int_{-\infty}^{\infty} A_{j_s}^*(\omega-\omega_2)H_j^*(\omega_2)e^{-i\omega_2t_2}d\omega_2 \tag{20}$$

Assuming $f_{i_r}(t)$ and $f_{j_s}(t)$ to be statistically independent between any two time segments, Equation (18) can be simplified to the following:

$$R_{z_iz_j}(t_1,t_2) = E[z_i(t_1)z_j(t_2)] = \sum_{r=1}^{n} E[z_{i_r}(t_1)z_{j_r}(t_2)] \tag{21}$$

where

$$E[z_{i_r}(t_1)z_{j_r}(t_2)] = \int_{-\infty}^{\infty} S_{f_{i_r}f_{j_r}}(\omega)I_{i_r}(t_1,\omega)I_{j_r}^*(t_2,\omega)d\omega \tag{22}$$

$I_{i_r}(t_1,\omega)$ can be obtained from Equations (15) and (19) by contour integration (Ref. 16). After some algebra, the final form is:

$$I_{i_r}(t_1,\omega) = \epsilon_r H_i(\omega) \cdot \left\{ u(t_1-t_{r-1}) \left[e^{i\omega t_1} - e^{i\omega t_{r-1}} \left(\psi_i(t_1-t_{r-1}) + i\frac{\omega}{\omega_{i_d}} \phi_i(t_1-t_{r-1}) \right) \right] \right. \tag{23}$$

$$\left. - u(t_1-t_r) \left[e^{i\omega t_1} - e^{i\omega t_r} \left(\psi_i(t_1-t_{r-1}) + i\frac{\omega}{\omega_{i_d}} \phi_i(t_1-t_r) \right) \right] \right\}$$

where

$$\omega_{i_d} = \sqrt{1-\zeta_i^2}\,\omega_{i_n}$$

is the damped natural frequency of the ith mode, and

$$\psi_i(t) = e^{-\zeta_i \omega_{i_n} t} \left(\cos \omega_{i_d} t + \zeta_i \frac{\omega_{i_n}}{\omega_{i_d}} \sin \omega_{i_d} t \right) \tag{24}$$

$$\phi_i(t) = e^{-\zeta_i \omega_{i_n} t} \sin \omega_{i_d} t \tag{25}$$

Similar expressions can be derived for $I_{j_r}(t_2,\omega)$ and hence $I_{j_r}^*(t_2,\omega)$. If an analytic expression for the power spectral density $S_{f_{i_r}f_{j_r}}(\omega)$ is specified, Equation (22) can be integrated by residue calculus. $I_{i_r}(t_1,\omega)I_{j_r}^*(t_2,\omega)$ can be determined from Equation (23) and it is given in Appendix A.

2.3 Approximate Representation of Buffet Loads on Wing

In the previous section, it is seen that the response of a wing to non-stationary buffet loads can be evaluated once the power spectral density $S_{f_{i_r}f_{j_r}}(\omega)$ in each time segment is known. Let $p_r(x,y,t)$ be the fluctuating pressure on the wing at the rth time segment. Here $p_r(x,y,t)$ is taken to be statistically stationary and is related to the function $f_{i_r}(t)$ in Equation (8) by the following expression:

$$f_{i_r}(t) = \frac{1}{\epsilon_r} \iint_{\substack{\text{wing} \\ \text{planform}}} \phi_i(x,y)p_r(x,y,t)dxdy \tag{26}$$

The power spectral density can be written as:

$$S_{f_{i_r}f_{j_r}}(\omega) = \frac{1}{\epsilon_r^2} \iiint \phi_i(x_1,y_1)\phi_j(x_2,y_2)S_{p_r}(x_1,y_1,x_2,y_2,\omega)dx_1\,dy_1\,dx_2\,dy_2 \tag{27}$$

where $S_{p_r}(x_1, y_1, x_2, y_2, \omega)$ is the cross power spectral density between points (x_1, y_1) and (x_2, y_2) (Fig. 1) in the rth time segment.

Following a method used by Schweiker and Davis (Ref. 22), and Davis (Ref. 24) for the study of the response of shells to aerodynamic noise, the wing is divided into a number of panels (Fig. 4). Approximation to the integral in Equation (27) is made by assuming the pressure at the centre of a panel to be representative of the pressure field at all points within that panel. That is, the pressure spectrum at any point is given by that at the centre of the panel. The pressure cross spectrum between two points on the same panel is taken to be equal to the pressure spectrum at the panel centre, while if they lie on different panels, it has the same value as the cross-spectrum between the centres of the two panels. Equation (27) can be simplified to the following:

$$S_{f_{i_r} f_{j_r}}(\omega) = \frac{1}{\epsilon_r^2} \sum_{k=1}^{K} \sum_{\ell=1}^{K} \int_{A_k} \int_{A_\ell} S_{p_r}(x_1, y_1 x_2, y_2, \omega) \phi_i(x_1, y_1) \quad \phi_j(x_2, y_2) dx_1 dy_1 dx_2 dy_2 \tag{28}$$

where K is the number of panels the wing is divided into, A_k and A_ℓ are the areas of the kth and ℓth panel respectively. Within the panel of area A_k, an average mode shape for any mode 'i' is taken as:

$$\bar{\phi}_i^k = \frac{1}{A_k} \int_{A_k} \phi_i(x,y) dA_k \tag{29}$$

If points (x_1, y_1) and (x_2, y_2) fall on the same panel, say the kth panel, $S_{p_r}(x_1, y_1, x_2, y_2, \omega)$ is written as $S_{p_r}^k(\omega)$. On the other hand, if points (x_1, y_1) and (x_2, y_2) lie on different panels, for example, the kth and ℓth panels, then $S_{p_r}(x_1, y_1, x_2, y_2, \omega)$ is represented by

$$S_{p_r}(x_1, y_1, x_2, y_2, \omega) = S_{p_r}^k(\omega) e^{-\delta_k r_{k\ell}} \tag{30}$$

where δ_k is the spatial decay coefficient measured at the point (x_k, y_k) and $r_{k\ell}$ is the distance between the centres of the kth of ℓth panels (Fig. 4).

Using Equations (29) and (30), Equation (28) can be rewritten as follows:

$$S_{f_{i_r} f_{j_r}}(\omega) = \frac{1}{\epsilon_r^2} \sum_{k=1}^{K} S_{p_r}^k(\omega) X^k \tag{31}$$

where

$$X^k = \bar{\phi}_i^k A_k \cdot \left\{ \bar{\phi}_j^k A_k + \sum_{\ell \neq k} \bar{\phi}_j^\ell A_\ell e^{-\delta_k r_{k\ell}} \right\} \tag{32}$$

Using Equations (31) and (32) to determine $S_{f_{i_r} f_{j_r}}(\omega)$, and upon substitution into Equation (22) and carrying out the integration, the expected value $E[z_i(t_1) z_j(t_2)]$ can be evaluated from Equation (21) using Equation (22).

For a given wing, $\bar{\phi}_i^k$ and $\bar{\phi}_j^k$ can be calculated along with A_k and $r_{k\ell}$ once the dimensions of the panels have been decided. $S_{p_r}^k(\omega)$ and δ_k are usually determined experimentally or are estimated based on available power spectral density and decay coefficient data on similar wings. There are certain forms of the pressure spectrum that enable the integral in Equation (22) to be evaluated analytically. The pressure at any point on the wing can be considered to be made up of contributions from a number of sources. These sources may arise from flow separations, wing leading edge and tip vortices and other disturbances characteristic of that particular wing geometry. Assuming that the pressure fluctuations of these sources are uncorrelated, $S_{p_r}^k(\omega)$ can be written in series form as:

$$S_{p_r}^k(\omega) = \sum_{m=1}^{M} S_{p_r}^{km}(\omega) \tag{33}$$

where M is the number of terms that give a good fit to the experimental data. Reference 21 shows that quite complex power spectral density curves can be derived from the series representation of Equation (33) using the correlated noise and exponential (commonly used in isotropic turbulence) froms of the power spectral density.

2 4 Mean Square Response of Wing Displacement for Given Input Power Spectra

From Equation (21), the expected value $E[z_i(t_1)z_j(t_2)]$ can be rewritten as:

$$E\left[z_i(t_1)z_j(t_2)\right] = E\left[z_{i_q}(t_1)z_{j_q}(t_2)\right] + \sum_{r=1}^{q-1} E\left[z_{i_r}(t_1)z_{j_r}(t_2)\right] \tag{34}$$

where $t_{q-1} \leqslant t_1 \leqslant t_q$ and $t_{q-1} \leqslant t_2 \leqslant t_q$. In other words, if t_1 and t_2 lies in the qth time segment, the expected value is given by the sum of $E[z_{i_q}(t_1)z_{i_q}(t_2)]$ at the qth segment and contributions from the r = 1 to q - 1 segments. The significance of writing $E[z_i(t_1)z_j(t_2)]$ in the form of Equation (34) will become clear later on when it is shown that the two terms on the right hand side of the equation are obtained from different expressions.

If $S_{p_r}^{km}(\omega)$ takes on the spectrum of a white noise, then Equation (33) can be written as:

$$S_{p_r}^k(\omega) = S_r^k = \text{constant} \tag{35}$$

Substituting Equations (31) and (35) into (22) yields

$$E\left[z_{i_r}(t_1)z_{j_r}(t_2)\right] = \frac{1}{\epsilon_r^2} \sum_{k=1}^{K} X^k \tilde{E}\left[z_{i_r}(t_1)z_{j_r}(t_2)\right] \tag{36}$$

where

$$\tilde{E}\left[z_{i_r}(t_1)z_{j_r}(t_2)\right] = \int_{-\infty}^{\infty} S_r^k I_{i_r}(t_1,\omega) I_{j_r}^*(t_2,\omega) d\omega \tag{37}$$

Equation (37) can be evaluated for $t_{r-1} \leqslant t_1 \leqslant t_r$, $t_{r-1} \leqslant t_2 \leqslant t_r$ using Equation (A1) of Appendix A, while Equation (A2) is used for $t_1 \geqslant t_r$, $t_2 \geqslant t_r$. The poles in the integrand are given by the term $H_i(\omega)H_j^*(\omega)$, and there are four of them in the ω-plane, namely, $\rho_1 = \omega_{i_d} + i\zeta_i\omega_{i_n}$, $\rho_2 = -\omega_{i_d} + i\zeta_i\omega_{i_n}$, $\rho_3 = \omega_{j_d} - i\zeta_j\omega_{j_n}$ and $\rho_4 = -\omega_{j_d} - i\zeta_j\omega_{j_n}$. Using residue calculus, the integrations can be performed by choosing the proper integrated paths. The resulting expressions for $\tilde{E}[z_{i_r}(t_1)z_{j_r}(t_2)]$ are given by Equations (B1) and (B2) in Appendix B.

The mean square response of the wing displacement is obtained from Equation (7) using Equation (34) after setting $t_1 = t_2 = t$. If Equations (36) and (37) are substituted into Equation (34) to obtain $E[z_i(t_1)z_j(t_2)]$, the resulting response is for a white noise pressure spectrum in each of the time segments.

To handle more complex buffet load spectra, the term $S_{p_r}^{km}(\omega)$ in Equation (33) can be written in the following form:

$$S_{p_r}^{km}(\omega) = \frac{S_r^{km}\,\alpha_r^{2\,km}\left(\alpha_r^{2\,km} + \beta_r^{2\,km} + \omega^2\right)}{\left[\alpha_r^{2\,km} + (\omega + \beta_r^{km})^2\right]\left[\alpha_r^{2\,km} + (\omega - \beta_r^{km})^2\right]} \tag{38}$$

which is the correlated noise power spectral density. Here S, α and β are constants, and the subscript 'r' denotes the rth time segment, the superscripts 'k' and 'm' denote the kth panel and the mth mode respectively. Note that if β_r^{km} is set equal to zero, the resulting expression is the same as that used in Reference 16 for power spectrum of the form used for isotropic turbulence.

Using Equations (31) and (33), Equation (22) becomes

$$E\left[z_{i_r}(t_1)z_{j_r}(t_2)\right] = \frac{1}{\epsilon_r^2}\sum_{k=1}^{K}\sum_{m=1}^{M} X^k\,\tilde{E}^{km}\left[z_{i_r}(t_1)z_{j_r}(t_2)\right] \tag{39}$$

where

$$\tilde{E}^{km}\left[z_{i_r}(t_1)z_{j_r}(t_2)\right] = \int_{-\infty}^{\infty} S_{p_r}^{km}(\omega)I_{i_r}(t_1,\omega)I_j^*(t_2,\omega)d\omega \tag{40}$$

Substituting Equations (A1) and (A2) into the above expression, and using Equation (38) for $S_{p_r}^{km}(\omega)$, $\tilde{E}^{km}[z_{i_r}(t_1)z_{j_r}(t_2)]$ for $t_{r-1} \leqslant t_1 \leqslant t_r$, $t_{r-1} \leqslant t_2 \leqslant t_r$ is given by Equation (C1). When $t_1 \geqslant t_r$, $t_2 \geqslant t_r$, the expected value is given in Equation (C2). The mean square value of the wing response is again given by Equations (7) and (34) with $t_1 = t_2 = t$ and using Equations (39) and (40) to obtain $E[z_{i_r}(t)z_{j_r}(t)]$.

2.5 Mean Square Response of Wing Acceleration for Given Input Power Spectra

An expression similar to that of Equation (7) can be written for the acceleration by simply replacing $z(x,y,t)$ with the second time derivative $\ddot{z}(x,y,t)$, that is,

$$E\left[\ddot{z}^2(x,y,t)\right] = \sum_{i=1}^{I}\sum_{j=1}^{I} \phi_i(x,y)\phi_j(x,y)E\left[\ddot{z}_i(t)\ddot{z}_j(t)\right] \tag{41}$$

$E[\ddot{z}_i(t)\ddot{z}_j(t)]$ is obtained from the following equation:

$$E\left[\ddot{z}_i(t)\ddot{z}_j(t)\right] = E\left[\ddot{z}_{i_q}(t)\ddot{z}_{j_q}(t)\right] + \sum_{r=1}^{q-1} E\left[\ddot{z}_{i_r}(t)\ddot{z}_{j_r}(t)\right] \tag{42}$$

where $t_{q-1} \leqslant t \leqslant t_q$. If the pressure fluctuations in each time segment have spectra of the white noise type, then:

$$E\left[\ddot{z}_{i_r}(t)\ddot{z}_{j_r}(t)\right] = \frac{1}{\epsilon_r^2}\sum_{k=1}^{K} X^k \tilde{E}\left[\ddot{z}_{i_r}(t)\ddot{z}_{j_r}(t)\right] \tag{43}$$

while for correlated noise power spectral density,

$$E\left[\ddot{z}_{i_r}(t)\ddot{z}_{j_r}(t)\right] = \frac{1}{\epsilon_r^2}\sum_{k=1}^{K}\sum_{m=1}^{M} X^k \tilde{E}^{km}\left[\ddot{z}_{i_r}(t)\ddot{z}_{j_r}(t)\right] \tag{44}$$

where
$$\tilde{E}\left[\ddot{z}_{i_r}(t)\ddot{z}_{j_r}(t)\right] = \frac{\partial^4}{\partial t_1^2 \partial t_2^2}\tilde{E}\left[z_{i_r}(t_1)z_{j_r}(t_2)\right]_{t_1=t_2=t} \tag{45}$$

and
$$\tilde{E}^{km}\left[\ddot{z}_{i_r}(t)\ddot{z}_{j_r}(t)\right] = \frac{\partial^4}{\partial t_1^2 \partial t_2^2}\tilde{E}^{km}\left[z_{i_r}(t_1)z_{j_r}(t_2)\right]_{t_1=t_2=t} \tag{46}$$

Using the equations given in Appendices B and C, Equations (45) and (46) can be evaluated by carrying out the differentiations and setting $t_1 = t_2 = t$. The resulting expressions are substituted into Equations (43) and (44). The mean square response of the acceleration of the wing is then determined from Equations (41) and (42). The expressions for $\tilde{E}[\ddot{z}_{i_r}(t)\ddot{z}_{j_r}(t)]$ are given in Appendix D, while those for $\tilde{E}^{km}[\ddot{z}_{i_r}(t)\ddot{z}_{j_r}(t)]$ are given in Appendix E.

2.6 Expressions for Displacement and Acceleration Response in Non-Dimensional Forms

It is convenient for computation purposes to express the equations derived in Sections 2.4 and 2.5 in non-dimensional forms. Consider first the case where the pressure power spectral densities are of the form for white noise. Panel 1 (k = 1) is taken as the reference panel and the subscript 'r_o' is used to present the conditions at $\epsilon(t) = 1$. Using the time segmentation technique (Fig. 3), $\Delta C_{p_{rms}}$ and the power spectral density curves given in Reference 9 are assumed to be the values at the time segment when the load intensity is at its maximum, that is, at $\epsilon_r = 1$. The relation between S_r^k at the rth time segment and its value at $\epsilon_r = 1$ is

$$S_r^k = \epsilon_r^2 S_{r_o}^k \tag{47}$$

Define the following non-dimensional quantities:

$$\bar{S}_r^k = \frac{S_r^k}{S_{r_o}^1} \tag{48}$$

$$\tilde{\phi}_i^k = \frac{\bar{\phi}_i^k}{\bar{\phi}_1^1} \tag{49}$$

$$\bar{\phi}_j^k = \frac{\bar{\phi}_j^k}{\bar{\phi}_1^1} \tag{50}$$

$$\bar{A}_k = \frac{A_k}{A_1} \tag{51}$$

$$\bar{\zeta}_i = \frac{\zeta_i}{\zeta_1} \tag{52}$$

$$\bar{M}_i = \frac{M_i}{M_1} \tag{53}$$

$$\bar{\omega}_{i_n} = \frac{\omega_{i_n}}{\omega_{1_n}} \tag{54}$$

In terms of $\bar{S}_{r_o}^k$, $\bar{S}_r^k$ can be written as:

$$\bar{S}_r^k = \epsilon_r^2 \, \bar{S}_{r_o}^k \tag{55}$$

and $\bar{S}_{r_o}^k$ can be expressed as:

$$\bar{S}_{r_o}^k = \left(\frac{\Delta C_{p_{rms}}^k}{\Delta C_{p_{rms}}^1} \right)^2 \tag{56}$$

From Equation (32), let

$$X^k = \bar{X}^k (\bar{\phi}_1^1)^2 A_1^2 \tag{57}$$

where $$\bar{X}^k = \tilde{\phi}_i^k \bar{A}_k \left\{ \tilde{\phi}_j^k \bar{A}_k + \sum_{\ell \neq k} \tilde{\phi}_j^\ell \bar{A}_\ell e^{-\delta k r_{k\ell}} \right\}$$

Substituting into Equation (36) and using either Equation (B1) or (B2) for $\tilde{E}[z_{i_r}(t_1)z_{j_r}(t_2)]$ yields the following expression for $E[z_{i_r}(t)z_{j_r}(t)]$:

$$E[z_{i_r}(t)z_{j_r}(t)] = \epsilon_r^2 (\bar{\phi}_1^1)^2 A_1^2 K S_{r_o}^1 \frac{\pi \Psi_a}{2\zeta_i M_i M_j \omega_{i_n}^3} \frac{1}{K} \sum_{k=1}^{K} \bar{X}^k \bar{S}_{r_o}^k \tag{58}$$

In deriving this expression, t_1 and t_2 have been set equal to t. Let $\bar{E}[z_{i_r}(t)z_{j_r}(t)]$ be the non-dimensional form of $E[z_{i_r}(t)z_{j_r}(t)]$ defined as:

$$\bar{E}[z_{i_r}(t)z_{j_r}(t)] = \frac{2\zeta_1 M_1^2 \omega_{1_n}^3}{\pi K (\bar{\phi}_1^1)^2 A_1^2 S_{r_o}^1} E[z_{i_r}(t)z_{j_r}(t)] \tag{59}$$

Then $\bar{E}[z_{i_r}(t)z_{j_r}(t)]$ can be expressed as:

$$\bar{E}[z_{i_r}(t)z_{j_r}(t)] = \frac{\epsilon_r^2 \Psi_a}{\bar{\zeta}_i \bar{M}_i \bar{M}_j \bar{\omega}_{i_n}^3} \frac{1}{K} \sum_{k=1}^{K} \bar{X}^k \bar{S}_{r_o}^k \tag{60}$$

where the expressions for Ψ_a for $t_{r-1} \leq t \leq t_r$, and $t \geq t_r$ are given in Appendix B. A similar equation can be derived from Equation (39) for correlated noise power spectral densities. Since it is assumed that the shapes of the power spectral density curves at different time segments are similar and differ in scale only, α_r^{km} and β_r^{km} in Equation (38) can be written in terms of the values at $\epsilon_r = 1$ as $\alpha_{r_o}^{km}$ and $\beta_{r_o}^{km}$ respectively.

Define

$$\tilde{S}_{r_o}^{km} = \frac{S_{r_o}^{km}}{S_{p_{r_o}}^k(0)} \tag{61}$$

and similar to Equation (47), let

$$\tilde{S}_r^{km} = \epsilon_r^2 \tilde{S}_{r_o}^{km} \tag{62}$$

Using Equation (39) and Equation (C1) for $t_{r-1} \leq t \leq t_r$, or Equation (C2) for $t \geq t_r$, $E[z_{i_r}(t)z_{j_r}(t)]$ can be written as:

$$E[z_{i_r}(t)z_{j_r}(t)] = \frac{\epsilon_r^2 \pi}{2\zeta_i M_i M_j \omega_{i_n}^3} \sum_{k=1}^{K} \sum_{m=1}^{M} X^k S_{r_o}^{km} \Psi_b \tag{63}$$

Using Equation (57), define

$$\tilde{X}^k = \left(\frac{\Delta C_{p_{rms}}^k}{\Delta C_{p_{rms}}^1} \right)^2 \frac{\bar{X}^k}{\pi \sum_{m=1}^{M} \tilde{S}_{r_o}^{km} \alpha_{r_o}^{km}} \tag{64}$$

and

$$S_o' = \pi (\bar{\phi}_1^1)^2 A_1^2 S_{p_{r_o}}^1 (0) \sum_{m=1}^{M} \tilde{S}_{r_o}^{1m} \alpha_{r_o}^{1m} \tag{65}$$

Similar to Equation (59), define a non-dimensional form for $E[z_{i_r}(t)z_{j_r}(t)]$ as follows:

$$\bar{E}[z_{i_r}(t)z_{j_r}(t)] = \frac{2\zeta_1 M_1^2 \omega_{1_n}^3}{\pi K S_o'} E[z_{i_r}(t)z_{j_r}(t)] \tag{66}$$

Combining Equations (63) to (66) yields.

$$\bar{E}[z_{i_r}(t)z_{j_r}(t)] = \frac{\epsilon_r^2}{\bar{\zeta}_i \bar{M}_i \bar{M}_j \bar{\omega}_{i_n}^3} \frac{1}{K} \sum_{k=1}^{K} \sum_{m=1}^{M} \tilde{X}^k \tilde{S}_{r_o}^{km} \Psi_b \tag{67}$$

The acceleration response for white noise form of pressure power spectral density can be obtained from Equation (42). If the non-dimensional form for $E[\ddot{z}_{i_r}(t)\ddot{z}_{j_r}(t)]$ is written as:

$$\bar{E}[\ddot{z}_{i_r}(t)\ddot{z}_{j_r}(t)] = \frac{2\zeta_1 M_1^2}{\omega_{1_n} \pi K (\bar{\phi}_1^1)^2 A_1^2 S_{r_o}^1} E[\ddot{z}_{i_r}(t)\ddot{z}_{j_r}(t)] \tag{68}$$

then using Equation (D1) for $t_{r-1} \leq t \leq t_r$, or Equation (D2) for $t \geq t_r$, it can be expressed as:

$$\bar{E}[\ddot{z}_{i_r}(t)\ddot{z}_{j_r}(t)] = \frac{\bar{\omega}_{i_n}}{\bar{\zeta}_i \bar{M}_i \bar{M}_j} \epsilon_r^2 \Psi_c \frac{1}{K} \sum_{k=1}^{K} \bar{X}^k \bar{S}_{r_o}^k \tag{69}$$

Corresponding to Equation (44) for correlated noise power spectral density, if $\bar{E}[\ddot{z}_{i_r}(t)\ddot{z}_{j_r}(t)]$ is defined as:

$$\bar{E}[\ddot{z}_{i_r}(t)\ddot{z}_{j_r}(t)] = \frac{2\zeta_1 M_1^2}{\alpha_{r_o}^{11}\pi K S_o} E[\ddot{z}_{i_r}(t)\ddot{z}_{j_r}(t)] \tag{70}$$

then using Equations (E1) or (E2) gives the following:

$$\bar{E}[\ddot{z}_{i_r}(t)\ddot{z}_{j_r}(t)] = \frac{\epsilon_r^2}{\bar{\zeta}_i \bar{M}_i \bar{M}_j} \frac{1}{K} \sum_{k=1}^{K} \sum_{m=1}^{M} \tilde{X}^k \tilde{S}_{r_o}^{km} \Psi_d \frac{\alpha_{r_o}^{km}}{\alpha_{r_o}^{11}} \tag{71}$$

where S_o' is given by Equation (65). With expressions $\bar{E}[z_{i_r}(t)z_{j_r}(t)]$ and $\bar{E}[\ddot{z}_{i_r}(t)\ddot{z}_{j_r}(t)]$ given by Equations (60) and (68), or Equations (67) and (71) for white noise or correlated noise form of power spectral densities of the pressure fluctuations respectively, the total displacement and acceleration response at any point on the wing can be obtained from Equations (7) and (41). Non-dimensional forms of the mean square response $\bar{E}[z^2(x,y,t)]$ or $\bar{E}[\ddot{z}^2(x,y,t)]$ can be obtained following the definitions of $\bar{E}[z_{i_r}(t)z_{j_r}(t)]$ and $\bar{E}[\ddot{z}_{i_r}(t)\ddot{z}_{j_r}(t)]$ given in Equations (59) and (66), or Equations (68) and (70) respectively.

3.0 AN ILLUSTRATIVE EXAMPLE

The steps involved in computing the response of the wing are fairly straightforward once the necessary aeroelastic data are given. As an example, the response of a F-4E wing is studied using the data supplied by Mullans and Lemley (Ref. 9). Figure 5 is taken from Reference 9 and shows the choice of panel dimensions on the wing. A total of eighteen panels (K = 18) are used in the computations, and the panel centres are marked numerically from 1 to 18. The distances between the centres of any two panels $r_{k\ell}$ can be determined from the geometry of the wing planform.

Only the first ten symmetrical modes are considered in this example. The natural frequencies ω_{i_n}, generalized mass M_i, average mode shape $\bar{\phi}_i^k$ and damping ratio ζ_i for dynamic pressure q = 470 psf are tubulated in Mullans and Lemley's report (Ref. 9). They also obtained buffet data from wind tunnel tests on a 10% scale rigid three dimensional model. For a clean wing with zero leading edge and trailing edge deflections, the rms pressure coefficients $\Delta C_{p_{rms}}$ on the wing are shown in Figure 6. In this particular example, $\Delta C_{p_{rms}}$ varies practically linearly along constant chord and span directions.

The power spectral densities of the pressure fluctuations at various points on the wing for Mach number 0.7 and angle of incidence 12° are also given in Reference 9. The transducers are not located exactly at the panel centres and there may be more than one transducer per panel, or, in some cases, none at all. Figure 7 indicates the transducers (numbers correspond to these given in Ref. 9) whose measured outputs are used to represent the fluctuating pressures on the panels where they are located.

The value of the spatial decay coefficient δ_k given in Equation (30) can be found from cross-correlation of the pressure fluctuations at two points on the wing. Its value is taken to be constant between any two points on different panels and equal to 0.25. The variation of the intensity of the input load with time is assumed to be sinusoidal, that is,

$$\epsilon(t) = \sin \pi \frac{t}{T_B} \tag{72}$$

where T_B is the time the aircraft spends in the buffet regime (Fig. 3). The values of $\Delta C_{p_{rms}}$ given in Figure 6 are taken to correspond to $\epsilon(t) = 1$, or when $t = T_B/2$. Furthermore, it is assumed that the normalized shapes of the pressure power spectral density curves with respect to its value at zero frequency at different panels are the same for all values of $\epsilon(t)$. In other words, varying $\epsilon(t)$ changes the magnitude of power spectra only, but the normalized values are the same for all time segments. This requires the flow field on the wing to be similar at all times during the buffet maneuver with changes only in the scale of the fluctuating pressure force. This should be viewed as a rough approximation only. A more complete representation requires measurements of $\Delta C_{p_{rms}}$ and the pressure power spectral densities on all panels at flight conditions which correspond to the value of ϵ_r under consideration.

4.0 RESULTS AND DISCUSSIONS

In the formulation given in the previous sections, the Mach number, angle of incidence and dynamic pressure do not appear explicitly in the equations defining the response of the wing. The input buffet data necessary for the computations are the $\Delta C_{p_{rms}}$ and the power spectral densities of the pressure fluctuations at each of the 18 panels for the time segment $\epsilon_r \approx 1$. The data used in this example at $\epsilon_r = 1$ correspond to those given by Mullans and Lemley (Ref. 9) for q = 470 psf, M = 0.7 and $\alpha = 12°$. The variation in the buffet load with time arises from changes in flight conditions, for example, changes in the angle of incidence. A sinusoidal variation of $\epsilon(t)$ is chosen for convenience in the computations, even though the time segmentation technique can be used for quite general buffet maneuvers.

The experimentally determined power spectral density curves are expressed in series form using Equations (33) and (38). The unknowns $S_{r_o}^{km}$, $\alpha_{r_o}^{km}$ and $\beta_{r_o}^{km}$ and the number of terms in the series are obtained by a curve fitting procedure using Powell's minimization algorithm (Ref. 25). Figure 8 shows a comparison between the curve fitted non-dimensional power spectral density $\tilde{S}_{p_{r_o}}^{k}(\omega)$ (k = 18) versus frequency ω for transducer 16 at panel 18 (Fig. 7) with the smoothed experimental data taken from Reference 9. It is seen that only three terms are necessary in Equation (33) to give a very good fit to the experimental data. The individual terms are plotted in Figure 9. Curve 'a' has the exponential form of power spectral density which is used commonly for isotropic turbulence, and has been investigated in detail in Reference 16. Curves 'b' and 'c' have power spectra of the correlated noise type which has been studied in Reference 20. On examining these curves, the pressure can be decomposed into three components: a fluctuating part due to flow separations with power spectral density represented approximately by the exponential form, and two convected vortices or disturbances with correlated noise power spectral densities. These convected vortices can be identified as the leading edge and wing tip vortices. In curve fitting the power spectral densities taken from Reference 9, it is found that three terms are needed at most. For some panels, two terms are sufficient.

The mean square displacement response $E[z^2(x,y,t)]$ given in Equation (7) can be written in non-dimensional form at a panel centre as:

$$\bar{E}^k[z^2(t)] = \sum_{i=1}^{I} \sum_{j=1}^{I} \bar{\phi}_i^k \bar{\phi}_j^k \bar{E}[z_i(t)z_j(t)] \tag{73}$$

$\bar{E}[z_i(t)z_j(t)]$ is obtained from Equation (34) by setting $t_1 = t_2 = t$ and using non-dimensional forms of the expected values. Consider ϵ_r to be constant, and without loss in generality, take $\epsilon_r = 1$. This is equivalent to the case of the wing response to one time segment only, and Equation (67) can be used in place of Equation (34) to evaluate $\bar{E}[z_i(t)z_j(t)]$. The term Ψ_b in Equation (C1) for $t_{r-1} \leq t \leq t_r$, after setting $t_1 = t_2 = t$, determine the response to step modulated buffet loads, while for $t \geq t_r$,

substitution of Equation (C2) into Equation (67) gives the decay to pulse modulated loads. The pulse duration is given by the time segment Δt_r, which is equal to $t_r - t_{r-1}$.

Figure 10 shows the response at the centre of panel 18 for $\epsilon_r = 1$ using the values of $\Delta C_{p_{rms}}$ and spectral information given in Reference 9. The superscript $'$ is used to denote that time is non-dimensionalized with respect to the undamped natural period of the first mode of vibration $T_1 = \frac{2\pi}{\omega_{1_n}}$. The mean square response is normalized with respect to $\bar{E}^k[z^2(t')]_{max}$, which is the maximum value obtained as $t' - t'_{r-1} \rightarrow \infty$. This maximum response is the sum of the responses from the ten individual symmetrical modes of vibration together with the contributions from the correlation terms between different modes. The magnitude of the correlation terms can be obtained from the difference between curves '1' and '2' which amounts to approximately 8% for $t' - t'_{r-1} \gg 1$. As expected, the first bending mode of vibration is the dominant one, but it only accounts for 55% of the total response. Because the damping is fairly large for this particular wing, the response reaches its maximum in approximately three undamped natural periods T_1 of the first mode. The oscillations in the response curves are relatively small as compared to those of Reference 16 for small values of damping.

The decay of the mean square displacement response at the centre of panel 18 after the exciting force has been withdrawn at time t'_r is shown in Figures 11 to 13 for three values of the pulse duration ($\Delta t'_r = 0.5$, 1 and 2). The shapes of curves are very similar for the three values of $\Delta t'_r$ shown. In less than three undamped natural periods T_1 of the first mode, the decay curve is practically zero. Comparison of curves '1' and '2' shows the correlation terms to be small, especially for increasing $\Delta t'_r$. The oscillating behaviour of the decay curves can be observed from these figures, but the amplitudes are much smaller than those shown in Reference 16 for small damping ratios.

Figure 14 shows the response to a step modulated input buffet load at the centre of panel 18 assuming white noise pressure power spectral densities for all the panels. In this case, Equation (60) is used in place of Equation (67). Comparison with Figure 10 shows the response curves to be nearly the same. Similar observations are also made when the decay curves given in Figures 15 to 17 are compared to Figures 11 to 13. It thus appears that approximating the power spectral densities of the fluctuating pressures in all the panels by that of a white noise, the shapes of the response and decay curves when one time segment is considered do not differ much from those computed using series representation of the experimentally determined power spectral densities. It has been shown in Reference 16 that for $m = 1$ and $\beta^{km}_{r_o} = 0$, the response and decay curves are similar to those with white noise power spectral densities if ω_{i_n} is small compared to $\alpha^{km}_{r_o}$. For $\beta^{km}_{r_o} \neq 0$, which corresponds to the case where the power spectral density is of the correlated noise type, the results presented in Reference 20 show that if ω_{i_n} is not near $\beta^{km}_{r_o}$, the response and decay curves for $\omega_{i_n}/\alpha^{km}_{r_o} \ll 1$ are similar to those obtained in Reference 16 using the white noise form of power spectral density. The series representation of the experimental data shows that values of $\beta^{km}_{r_o}$ ($m \geq 2$) are large compared to the first few natural frequencies of the modes that contribute significantly to the response and decay. Also, at those panels where values of $\Delta C_{p_{rms}}$ are large, $\omega_{i_n} < \alpha^{km}_{r_o}$ for the lower modes. Hence, the use of white noise power spectral densities for the pressure fluctuations is a fairly good approximation for this particular example. It should also be noted that the computation time using white noise representation is significantly less than that using series representation. A comparison between Equations (60) and (67) shows that Ψ_b has to be computed $\sum_{k=1}^{K} M_k$ times, where M_k is the number of terms required in the series expression for $S^k_{p_{r_o}}(\omega)$ in the kth panel, while in Equation (60), Ψ_a needs to be evaluated only once.

Figure 18 shows the maximum displacement response ($t' - t'_{r-1} \to \infty$) normalized with respect to that at panel 18 for all the panels. The numerals 1 to 18 designate the panel centres, and their locations are given by $\bar{y}/b$. Here b is the semi-span, and $\bar{y}$ is the distance measured from the wing root along a constant percentage chord line (Fig. 5). As expected, the response increases in the outboard direction, and is larger for panels near the trailing edge than those close to the leading edge.

For an input buffet load with sinusoidal variation of ϵ with time, the displacement response versus time t' is shown in Figure 19. The results are for panel 18 using white noise pressure power spectral densities for all the panels. The duration of the applied load T'_B is forty times the natural period T_1 for the first vibration mode. Two cases are given for $\Delta t'_r = 0.5$ and 2, which correspond to eighty and twenty time segments respectively. Similar to Reference 16, it has been found that changing the number of time segments produces practically no differences in the computed results if $\Delta t'_r < 0.5$. In all subsequent computations, $\Delta t'_r$ is taken to be 0.5.

It has been shown in Reference 16 that for rapid maneuvers, that is, T'_B is small, the maximum response lags the applied load, and the amplitude is lower than that obtained if T'_B is very long. Since the damping for the wing in this example is fairly large, the lag is found to be negligibly small. The displacement amplitude decrement, which is defined as

$$\delta = \frac{\bar{E}^k[z^2(t')]_{\text{max. for } T'_B \to \infty} - \bar{E}^k[z^2(t')]_{\max}}{\bar{E}^k[z^2(t')]_{\text{max. for } T'_B \to \infty}} \times 100\% \tag{74}$$

is plotted versus T'_B in Figure 20 for panel 18. δ decreases sharply with T'_B initially, and it is less than 1% after 14 periods of vibration in the first mode.

The mean square acceleration response to step and pulse modulated buffet loads has been computed using an expression similar to Equation (73) with $z(t)$ replaced by $\ddot{z}(t)$. Comparing the results sults for white noise and those using series representation for the experimental pressure power spectral densities yields similar conclusions as with the displacement response. Only the white noise power spectral densities results are presented in this report, and they are shown in Figures 21 and 22 for panel 18. The results indicate that the response reaches its maximum value in less than one natural period T_1 of the first mode. The contributions from the correlation terms are larger than those for the displacement response, reaching a value of nearly 20% of $\bar{E}^k[\ddot{z}^2(t')]_{\max}$.

The decay curves in Figure 22 are shown for two values of the duration of the time segment ($\Delta t'_r = 0.5$ and 1). The curves reach practically zero value for $t' - t'_r \simeq 1$. As in the response case, the correlation terms between modes are more significant than those found for the displacement. For the two values of $\Delta t'_r$ shown in the figure, the curves are practically identical. The mean square acceleration response with sinsoidal variation of ϵ with time is shown in Figure 23 for $T'_B = 40$, $\Delta t'_r = 0.5$. For the same value of $\Delta t'_r$, Figure 19 shows the oscillations in the displacement response curve to be much smaller.

5.0 CONCLUSIONS

A method for predicting the mean square displacement and acceleration response of a wing to non-stationary buffet loads has been developed and applied to an example using available data for the F-4E wing. The time segmentation technique, which is an approximation to a continuously varying load with time, gives results which are practically independent of the duration of the time segment when it is below a certain minimum value. In this particular example, the minimum value is found to be about half the undamped natural period of the first vibration mode.

The present method of modelling the buffet load on the wing may overestimate the response, since the pressure cross-spectrum between two points on the same panel is taken to be equal to the pressure spectrum at the panel centre. Also, for two points lying on different panels, it has the same value as the cross-spectrum between the centres of the two panels. This simplification is probably admissible in providing approximate response data in the early stages of aircraft design, since detailed correlation measurements are extremely time consuming and expensive to carry out.

The complex experimental buffet pressure spectra can be expressed in the form of a series by a curve fitting procedure. The pressure can be decomposed into components. It is found that for all panels, the first term in the series representation gives the exponential form of power spectral density, which can be considered to be a fair approximation for separated flows. Other terms indicate the presence of convected vortices, and the number of such vortices depends on the location of the panel. In this particular example, it is found that approximating the pressure power spectral densities at each panel by that of a white noise yields results which are fairly close to those obtained using the experimentally measured values.

A significant portion of the wing response can be accounted for by the first few lower vibration modes. The correlation between modes, which are considered to be statistically dependent, is investigated and found to contribute less than 10% to the total mean square displacement response. For the acceleration response, the correlation terms are nearly 20% of the total.

A sinusoidal variation of load intensity with time is used as an example to demonstrate the computation of the response for the particular wing under investigation. Since the damping for this wing is fairly large, the lag between the maximum response and the applied load is negligibly small. The displacement amplitude decrement is practically zero after a few undamped natural periods of the first vibration mode.

6.0 REFERENCES

1. Liepman, H.W. — *On the Application of Statistical Concepts to the Buffeting Problems.* Journal Aeronautical Sciences, Vol. 19, No. 12, December 1952, pp. 793-800.

2. Liepman, H.W. — *Extension of the Statistical Approach to Buffeting and Gust Response of Wings of Finite Span.* Journal Aeronautical Sciences, Vol. 22, No. 3, March 1955, pp. 197-200.

3. Ribner, H.S. — *Spectral Theory of Buffeting and Gust Response: Unification and Extension.* Journal Aeronautical Sciences, Vol. 23, No. 12, December 1956, pp. 1075-1077.

4. Huston, W.B. Skopinski, T.H. — *Measurement and Analysis of Wing and Tail Buffeting Loads in a Fighter Airplane.* National Advisory Committee for Aeronautics, Report 1219, 1955.

5. Huston, W.B. Skopinski, T.H. — *Probability and Frequency Characteristics of Some Flight Buffet Loads.* National Advisory Committee for Aeronautics, Technical Note 3733, 1956.

6. Huston, W.B. — *A Study of the Correlation Between Flight and Wind Tunnel Buffet Loads.* North Atlantic Treaty Organization for Aeronautical Research and Development, Report 111, April—May 1957.

7. Skopinski, T.H.
Huston, W.B.
A Semi-Empirical Procedure for Estimating Wing Buffet Loads in the Transonic Region.
National Advisory Committee for Aeronautics, RML56E01, September 1956.

8. Davis, D.D.
Wornom, D.E.
Buffet Tests of an Attack-Airplane Model with Emphasis on Analysis of Data from Wind-Tunnel Tests.
National Advisory Committee for Aeronautics, RML57H13, February 1958.

9. Mullans, R.E.
Lemley, C.E.
Buffet Dynamic Loads During Transonic Maneuvers.
Air Force Flight Dynamics Laboratory, Technical Report AFFDL-TR-72-46, September 1972.

10. Hwang, C.
Pi, W.S.
Transonic Buffet Behaviour of Northrop F-5A Aircraft.
American Institute of Aeronautics and Astronautics, Paper 75-70, January 1975.

11. Hwang, C.
Pi, W.S.
Investigation of Steady and Fluctuating Pressure Associated with the Transonic Buffeting and Wing rock of a One-Seventh Scale Model of the F-5A Aircraft.
National Aeronautical and Space Administration, CR-3061, November 1978.

12. Cunningham, A.M. Jr.
Benepe, D.B.
Watts, D.
Waner, P.G.
A Method of Predicting Full Scale Buffet Response with Rigid Wind Tunnel Model Fluctuating Pressure Data. Vol. I: Prediction Method Development and Assessment.
National Aeronautical and Space Administration, CR-3035, November 1978.

13. Jones, J.G.
A Survey of the Dynamic Analysis of Buffeting and Related Phenomenon.
Royal Aircraft Establishment Technical Report 72197, February 1973.

14. Butler, G.F.
Spavins, G.R.
Preliminary Evaluation of a Technique for Predicting Buffet Loads in Flight from Wind-Tunnel Measurements on Models of Conventional Construction.
North Atlantic Treaty Organisation, Advisory Group for Aerospace Research and Development, Paper 23 of AGARD CP-204, 1976.

15. Zbrozek, J.K.
Jones, J.G.
Transient Buffet Loads on Wings.
Journal Sound Vibration, Vol. 5, No. 2, 1967, pp. 197-214.

16. Lee, B.H.K.
Theoretical Analysis of the Transient Response of a Wing to Non-Stationary Buffet Loads.
National Research Council Canada, LR-597, April 1979.

17. Caughey, T.K.
Stumpf, H.J.
Transient Response of a Dynamic System Under Random Excitation.
Transactions ASME, Series E: Journal of Applied Mechanics, Vol. 28, No. 4, December 1961, pp. 563-566.

18. Barnoski, R.L.
Maurer, J.R.
Mean-Square Response of Simple Mechanical Systems to Non-Stationary Random Excitation.
Transactions ASME, Series E: Journal of Applied Mechanics, Vol. 36, No. 12, June 1969, pp. 221-227.

19. Holman, R.E.
Hart, G.C.
Non-Stationary Response of Structural Systems.
ASCE Journal of Engineering Mechanics Division, Vol. 100, No. EM2, April 1974, pp. 415-431.

20. Lee, B.H.K.
A Theoretical Study of the Response of a Wing to Quasi-Stationary Correlated Noise Inputs.
National Research Council Canada, LTR-HA-38, May 1979.

21. Lee, B.H.K.
Multi-Modal Response of a Wing to Non-Stationary Loads Using a Time Segmentation Technique.
National Research Council Canada, LTR-HA-41, June 1979.

22. Schweiker, J.W.
Davis, R.E.
Response of Complex Shell Structures to Aerodynamic Noise.
National Aeronautics and Space Administration, CR-450, April 1966.

23. Bendat, J.S.
Piersol, A.G.
Random Data: Analysis and Measurement Procedures.
Wiley-Interscience, 1971.

24. Davis, R.E.
Random Pressure Excitation of Shells and Statistical Dependence Effect of Normal Mode Response.
National Aeronautics and Space Administration, CR-311, September 1965.

25. Powell, M.J.D.
A Method of Minimizing a Sum of Squares of Non-Linear Functions Without Calculating Derivatives.
Computer Journal, Vol. 7, No. 4, 1965, pp. 303-307.

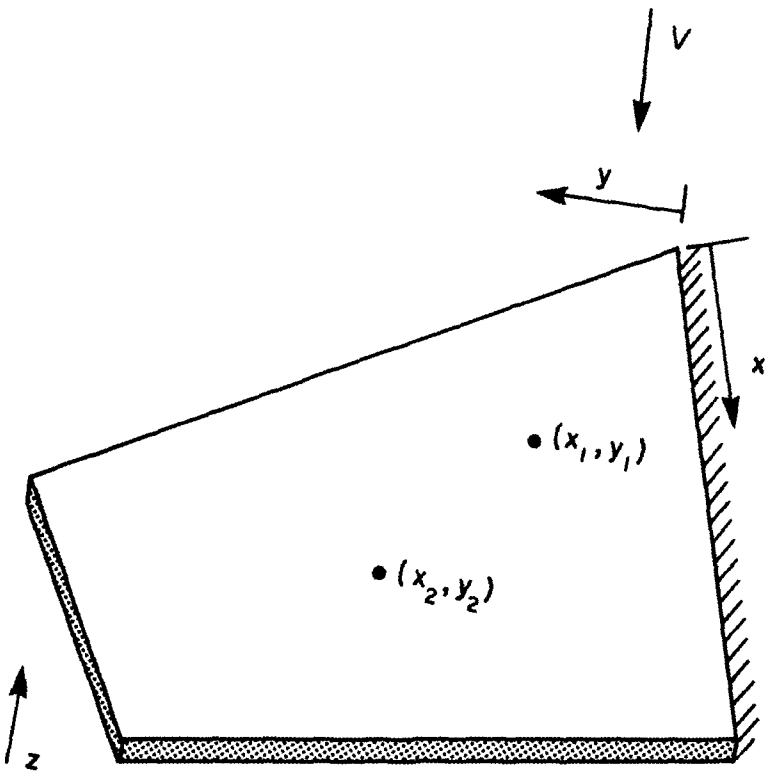

FIG. 1: SCHEMATIC OF WING

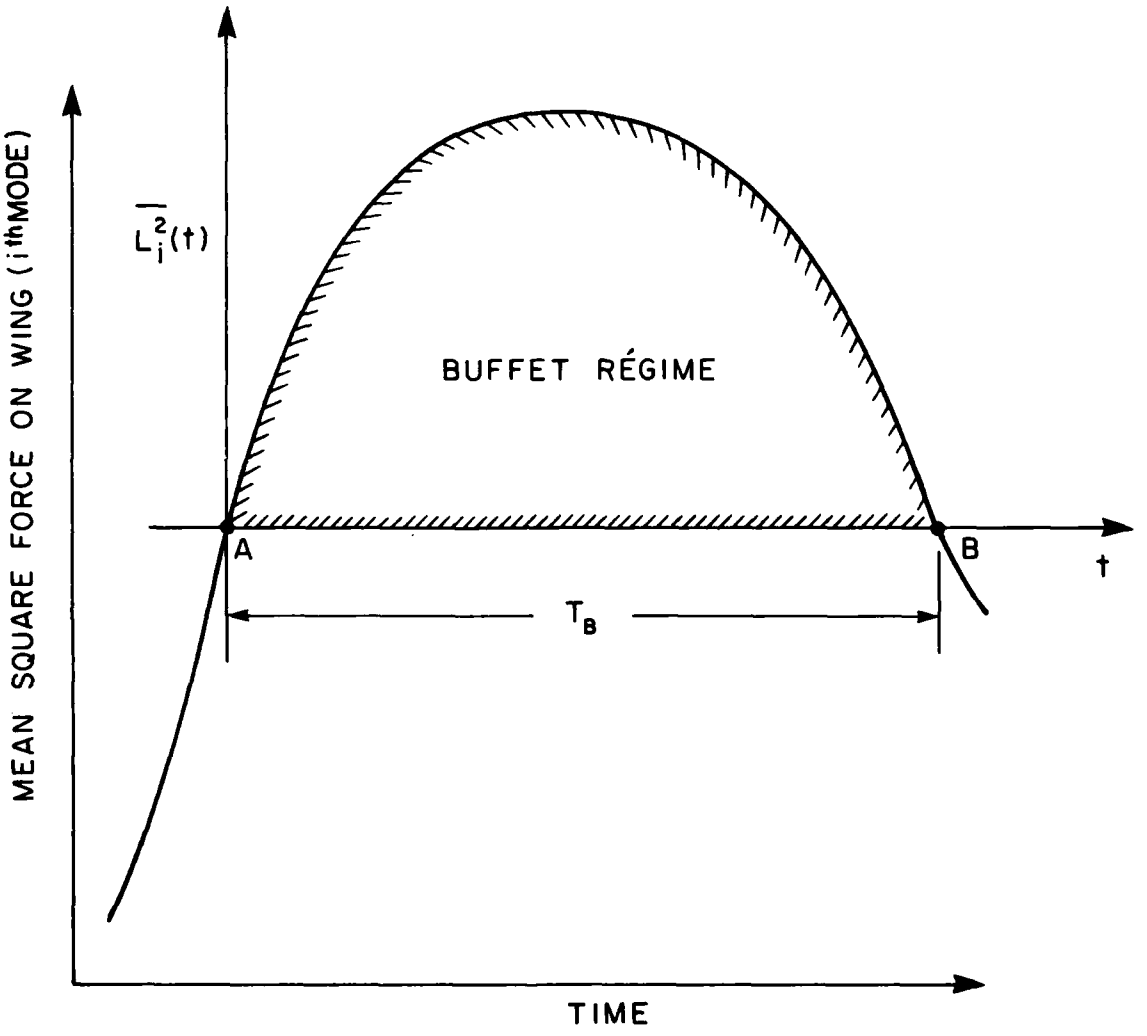

FIG. 2: SCHEMATIC ILLUSTRATING MEAN SQUARE LOADING ON WING VERSUS TIME

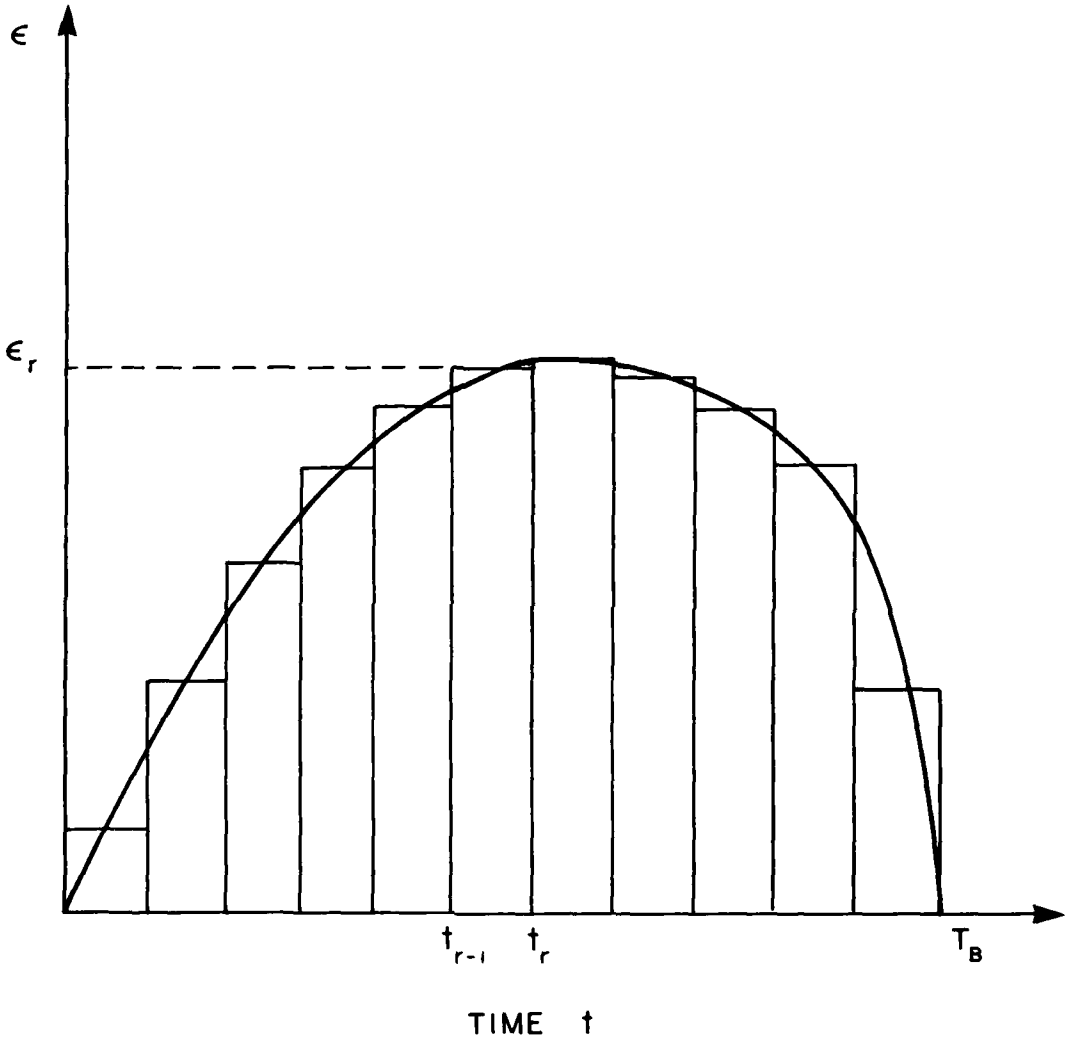

FIG. 3: SCHEMATIC SHOWING VARIATION OF ϵ WITH TIME

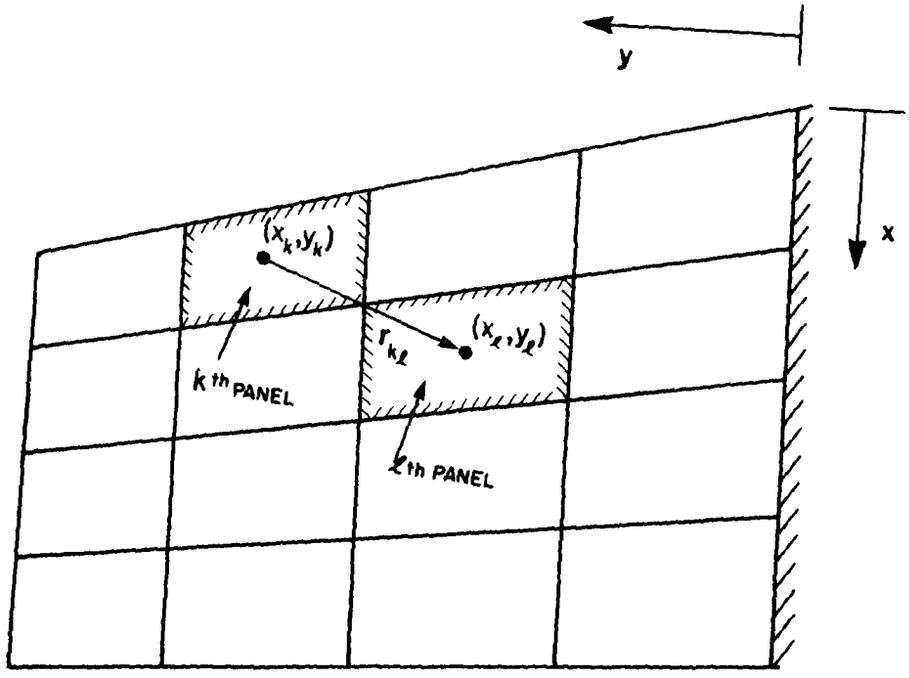

FIG. 4: PANEL REPRESENTATION OF WING

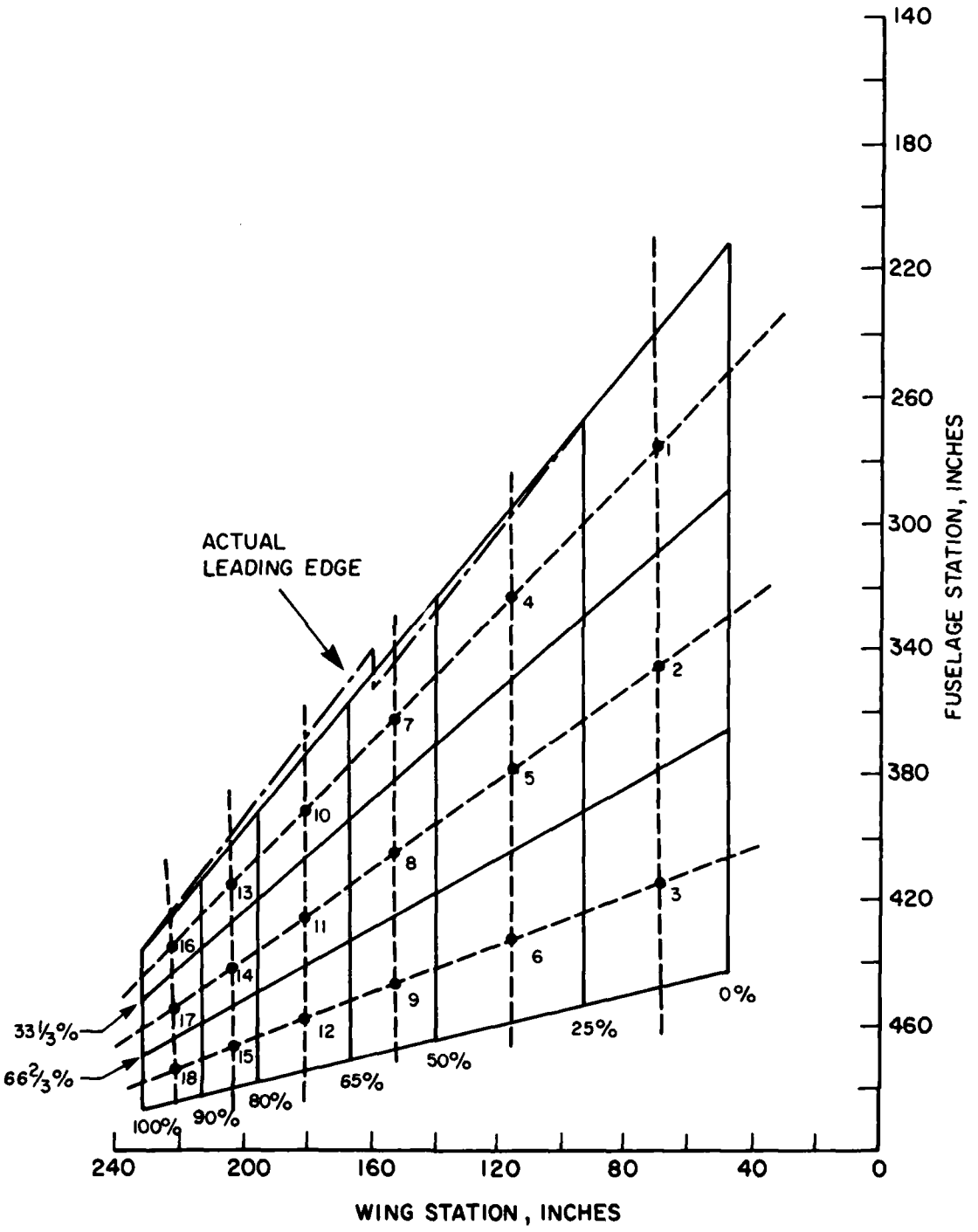

FIG. 5: PANEL REPRESENTATION OF F-4E WING PLANFORM

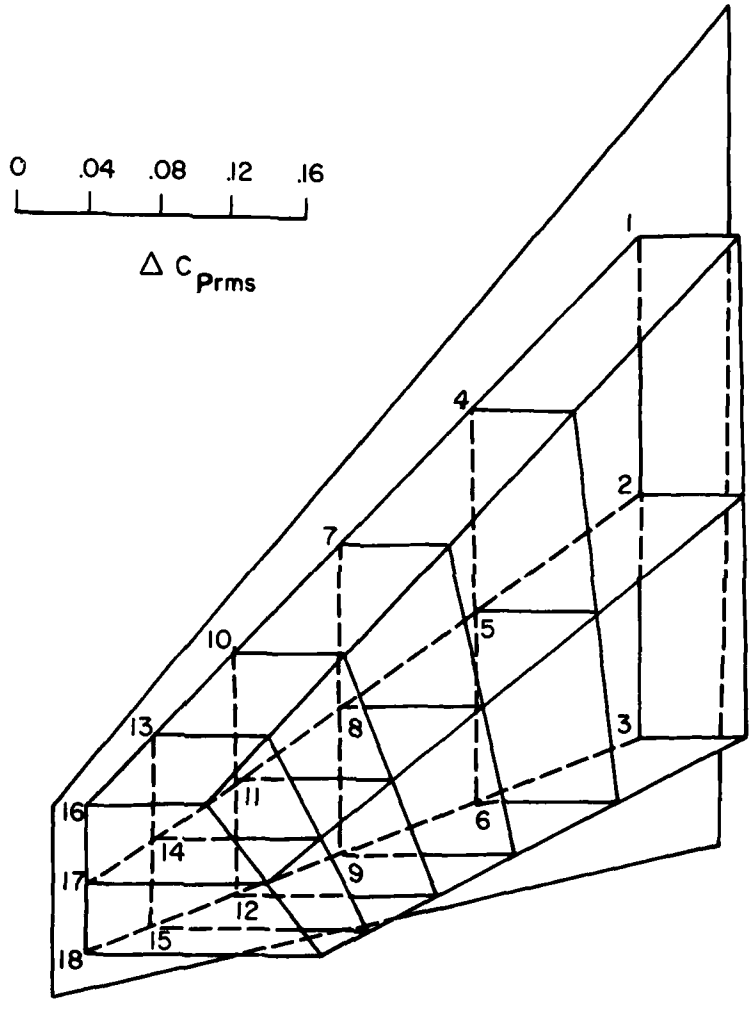

FIG. 6: APPROXIMATE MODELLING OF RMS PRESSURE COEFFICIENT ON WING

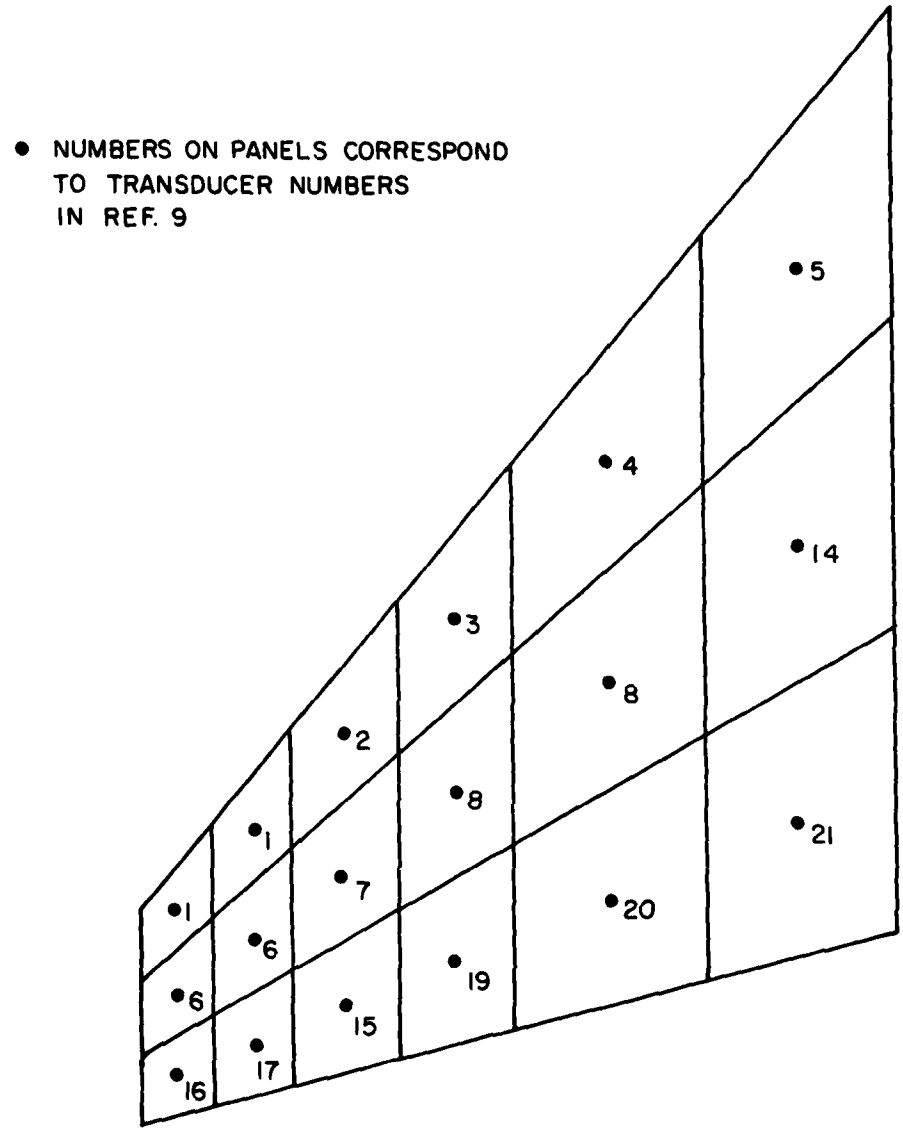

FIG. 7: PRESSURE TRANSDUCER LOCATIONS

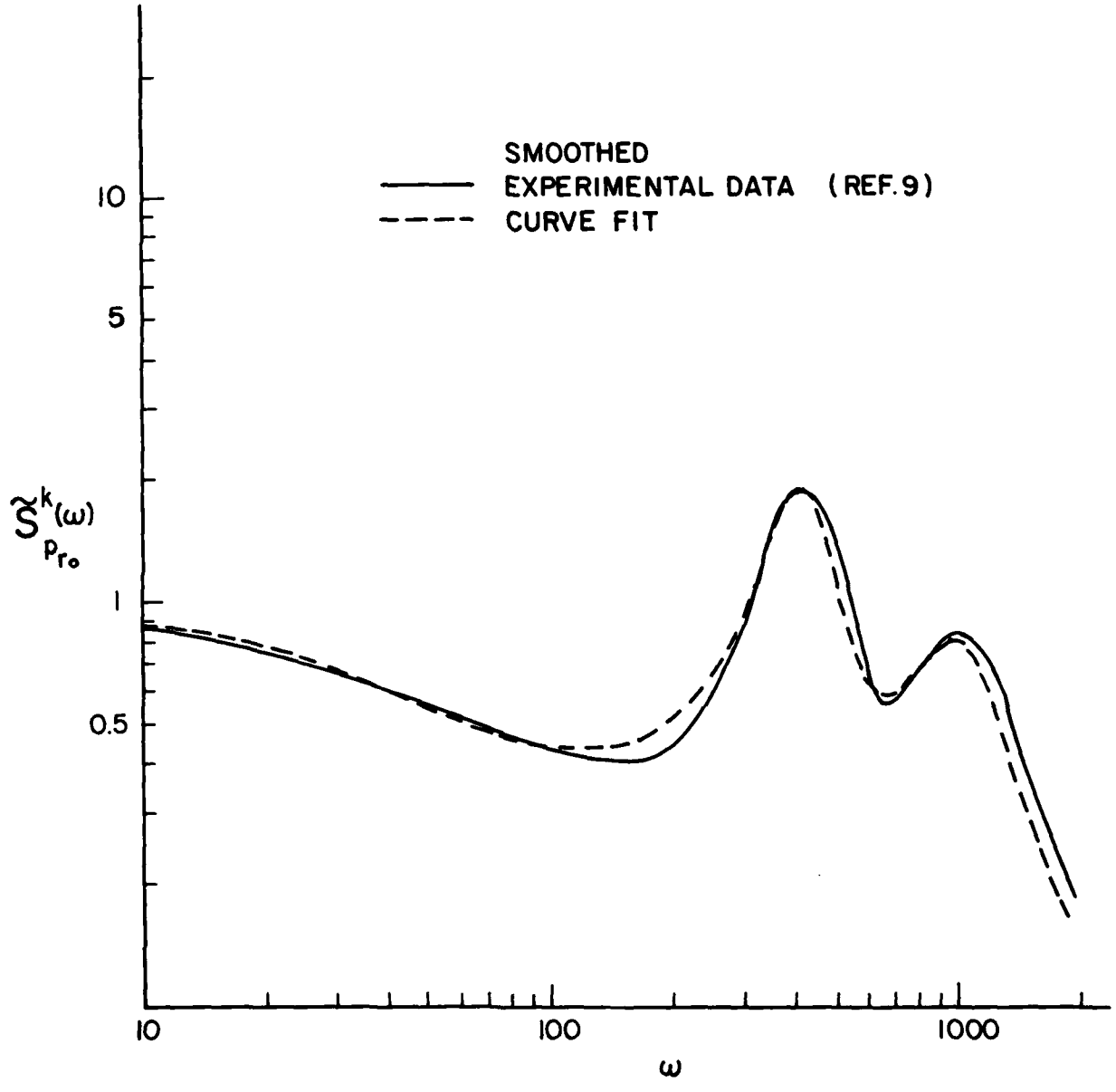

FIG. 8: PRESSURE POWER SPECTRAL DENSITY AT CENTRE OF PANEL 18

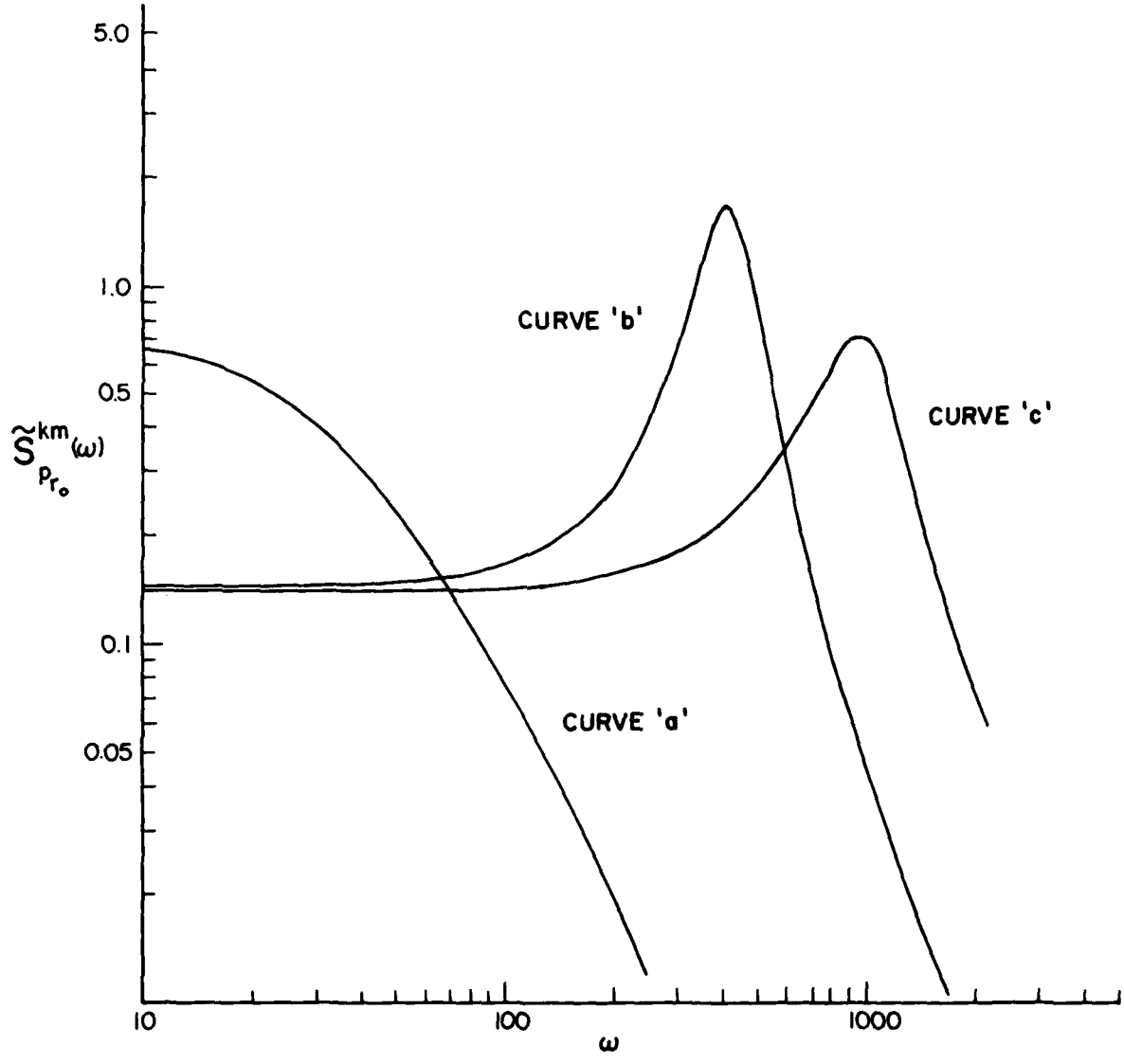

FIG. 9. PRESSURE POWER SPECTRAL DENSITIES OF THE THREE TERMS IN THE SERIES REPRESENTATION OF THE EXPERIMENTAL DATA FOR THE FLUCTUATING PRESSURE AT PANEL 18

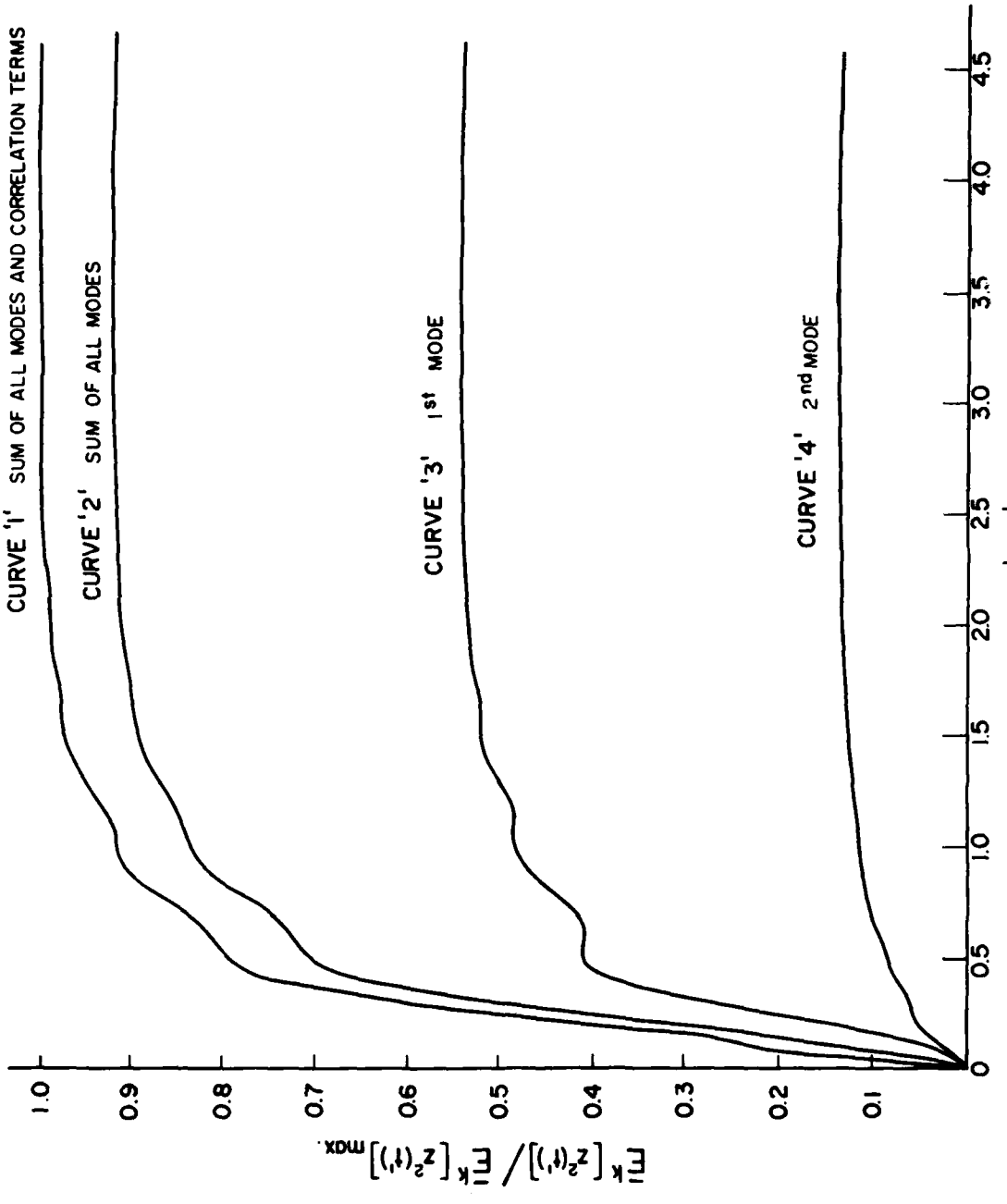

FIG. 10: RESPONSE TO A STEP MODULATED BUFFET LOAD AT THE CENTRE OF PANEL 18

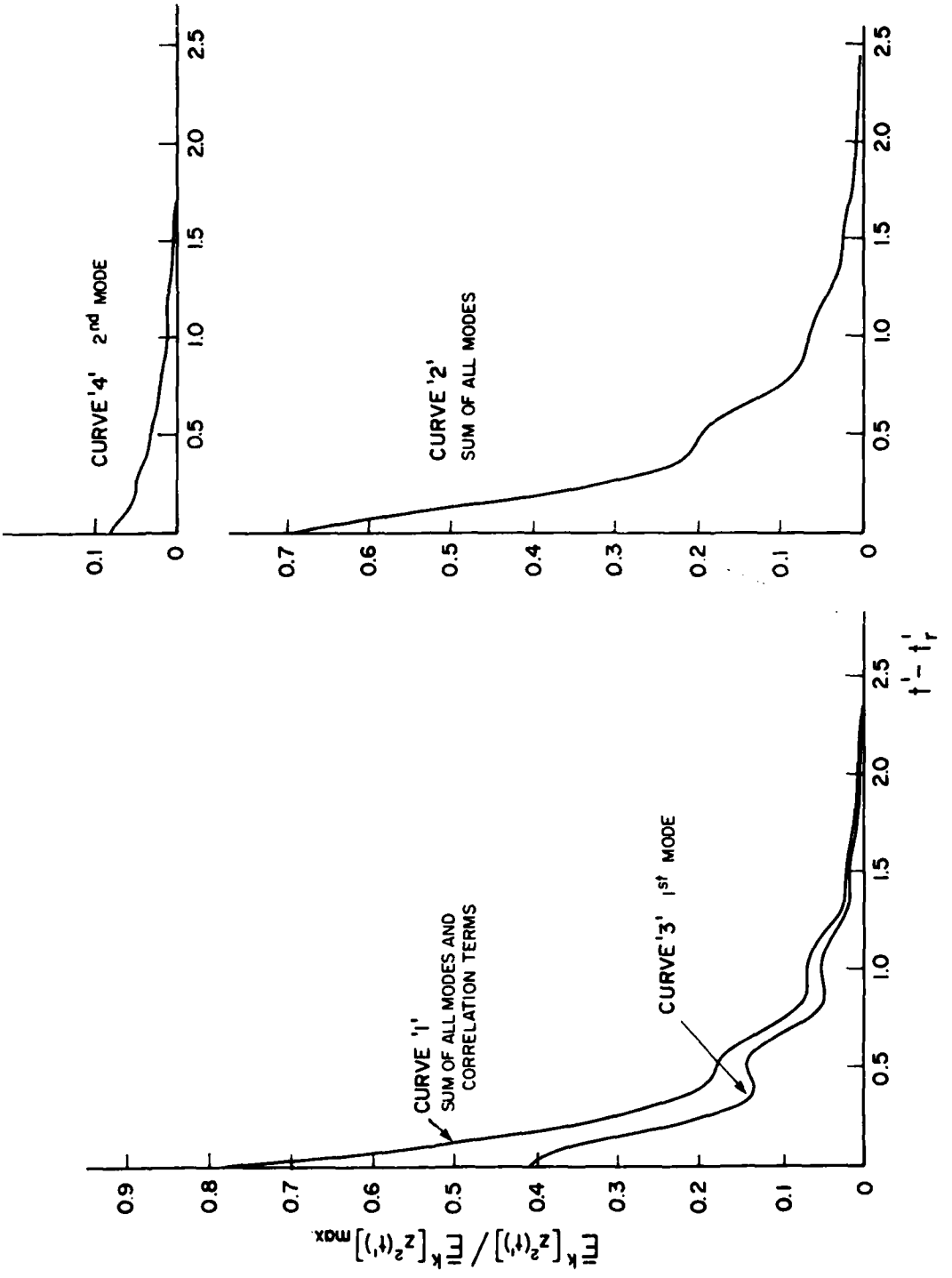

FIG. 11: DECAY TO A PULSE MODULATED BUFFET LOAD AT CENTRE OF PANEL 18 FOR $\Delta t'_r = 0.5$

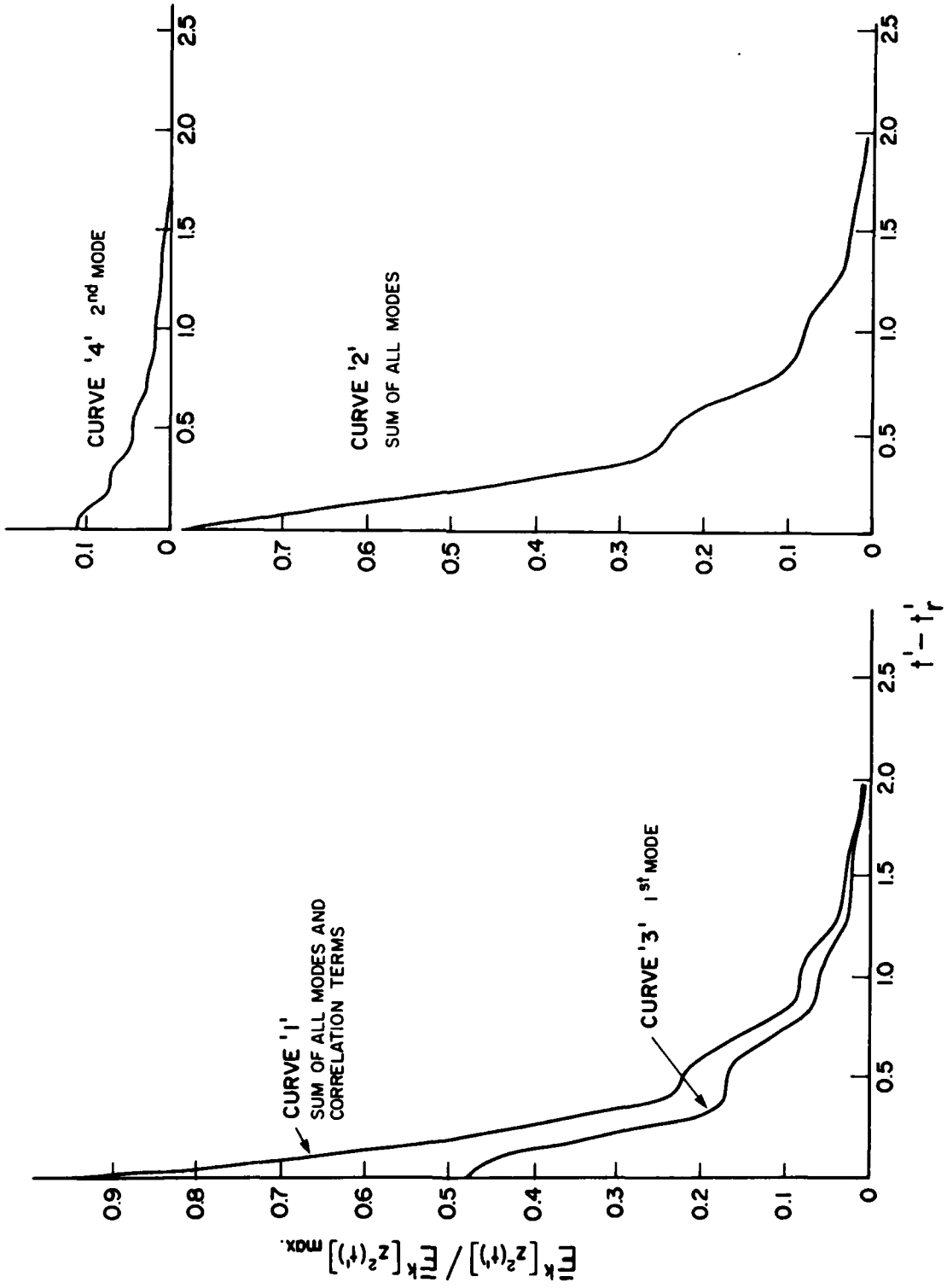

FIG. 12: DECAY TO A PULSE MODULATED BUFFET LOAD AT CENTRE OF PANEL 18 FOR $\Delta t_r' = 1.0$

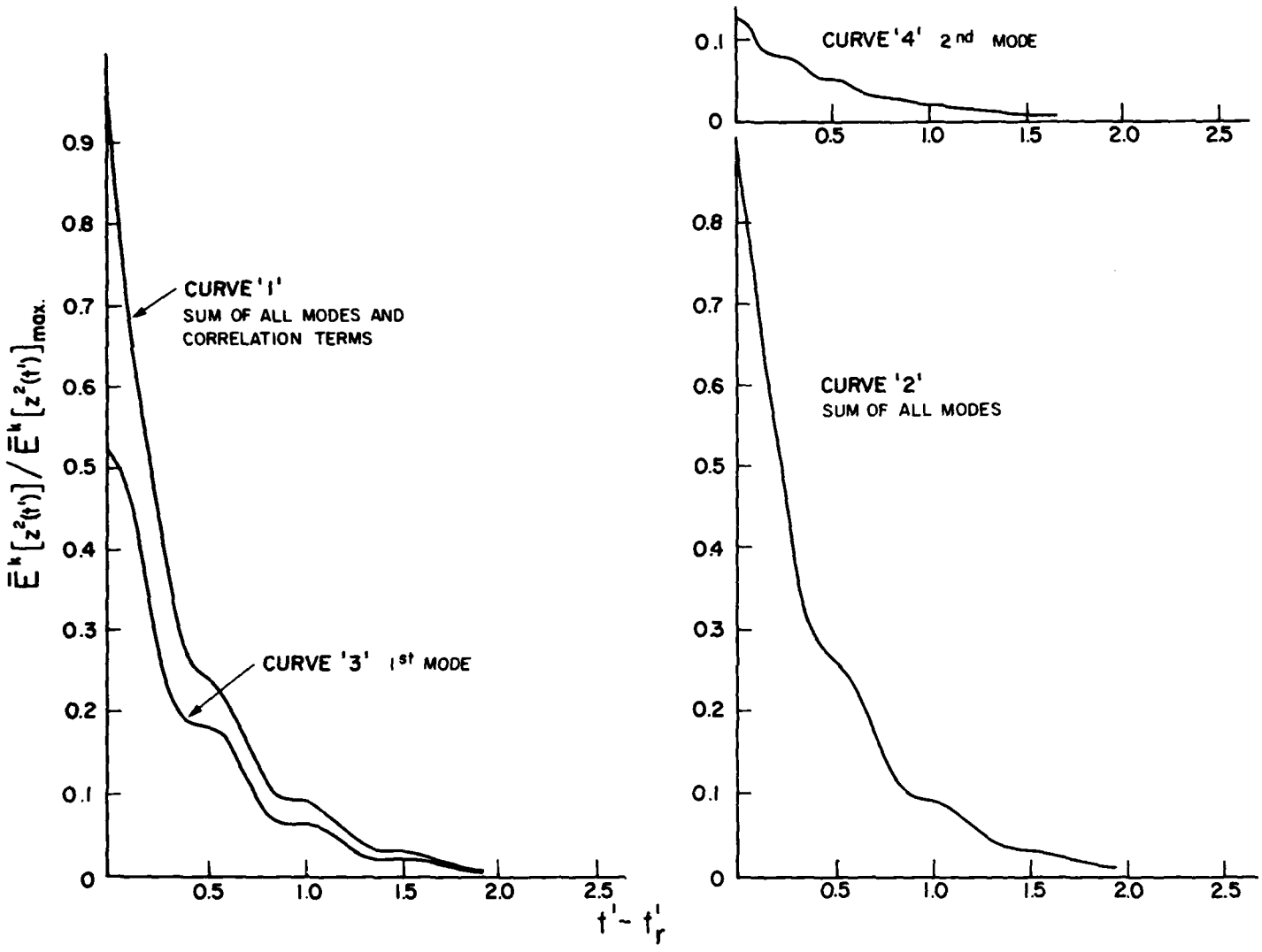

FIG. 13: DECAY TO A PULSE MODULATED BUFFET LOAD AT CENTRE OF PANEL 18 FOR $\Delta t'_r = 2.0$

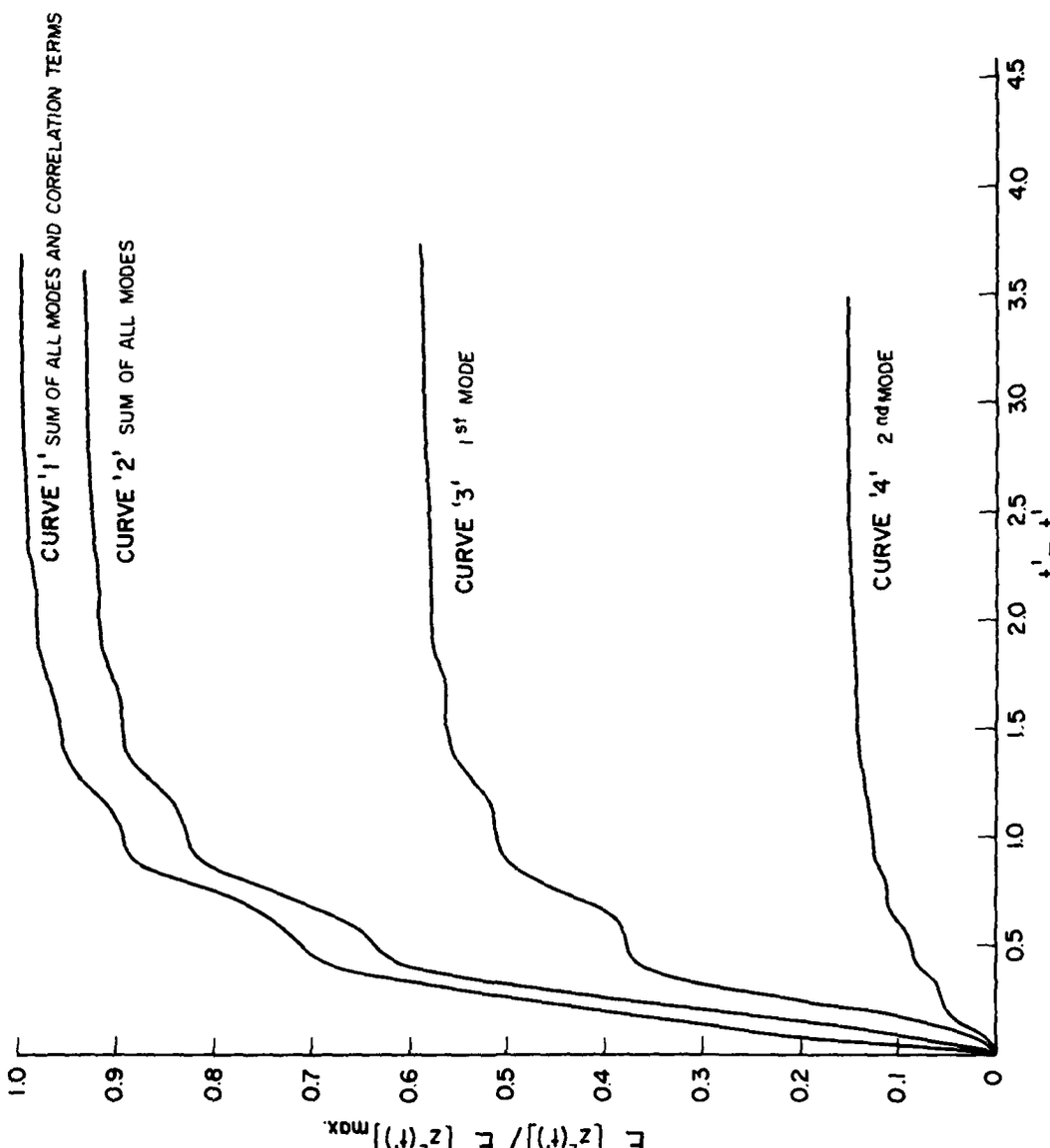

FIG. 14: RESPONSE TO A STEP MODULATED BUFFET LOAD AT CENTRE OF PANEL 18 FOR WHITE NOISE PRESSURE POWER SPECTRAL DENSITIES

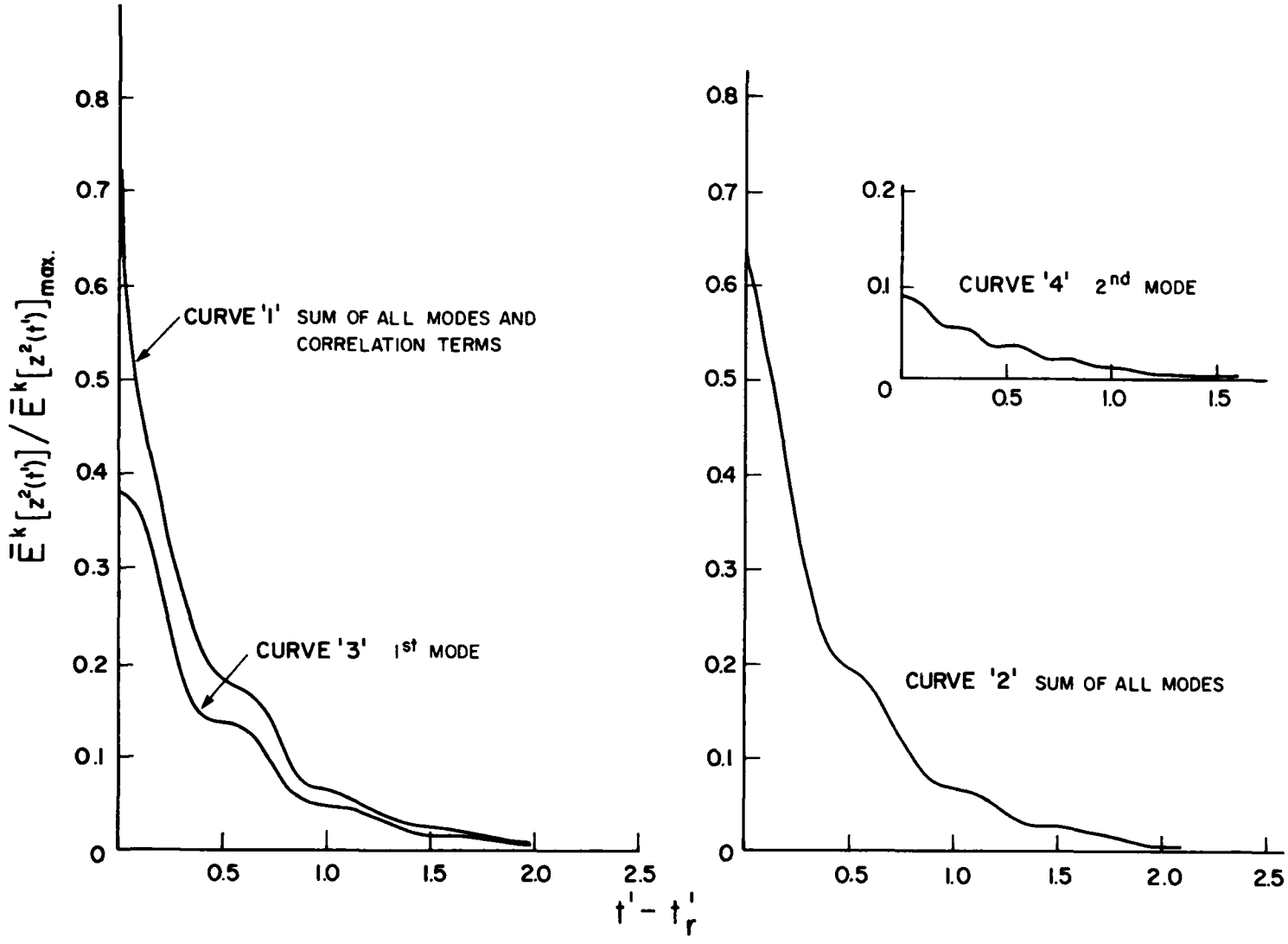

FIG. 15: DECAY TO PULSE MODULATED BUFFET LOAD AT CENTRE OF PANEL 18 FOR WHITE NOISE PRESSURE POWER SPECTRAL DENSITIES ($\Delta t'_r$ = 0.5)

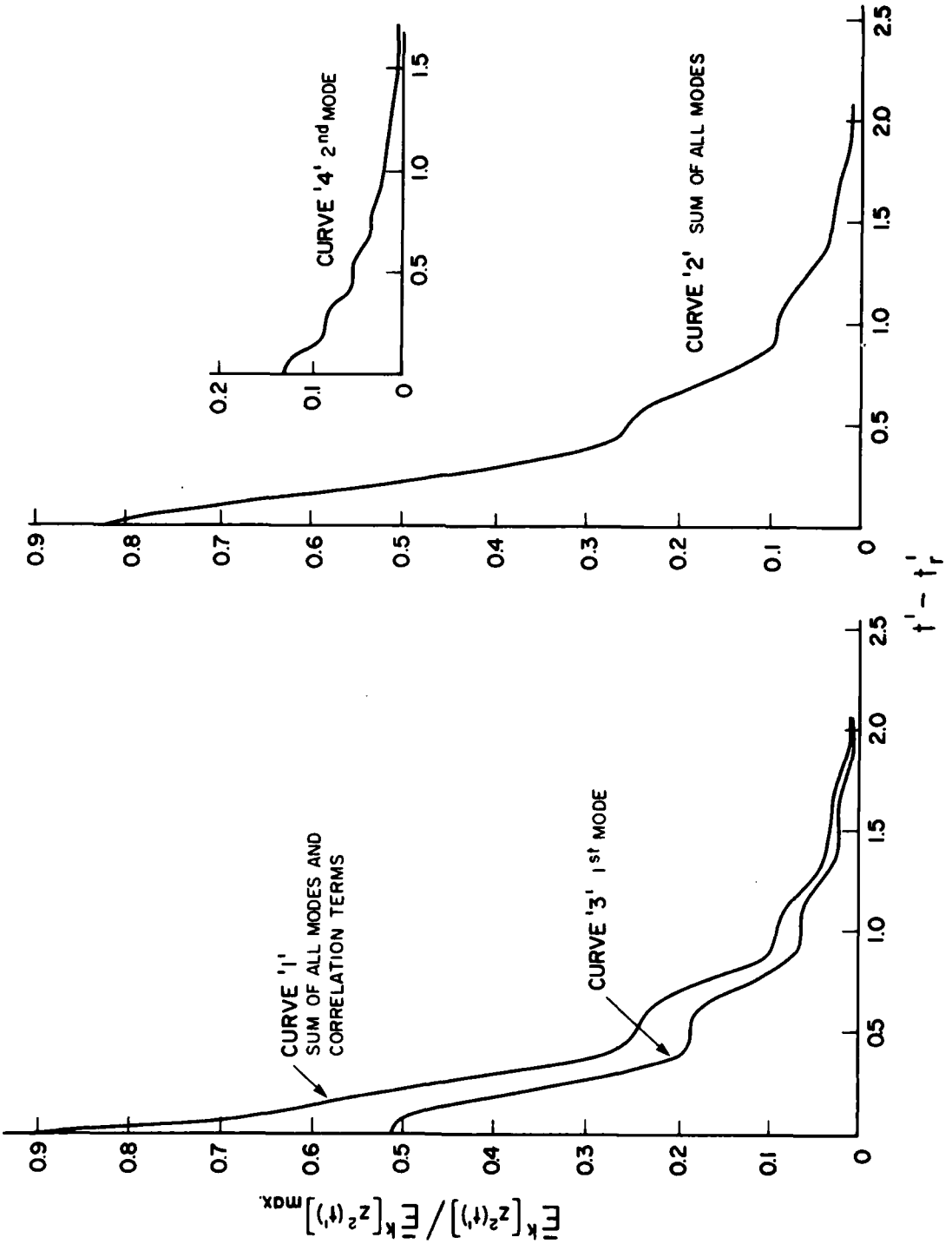

FIG. 16: DECAY TO PULSE MODULATED BUFFET LOAD AT CENTRE OF PANEL 18
FOR WHITE NOISE PRESSURE POWER SPECTRAL DENSITIES ($\Delta t_r' = 1.0$)

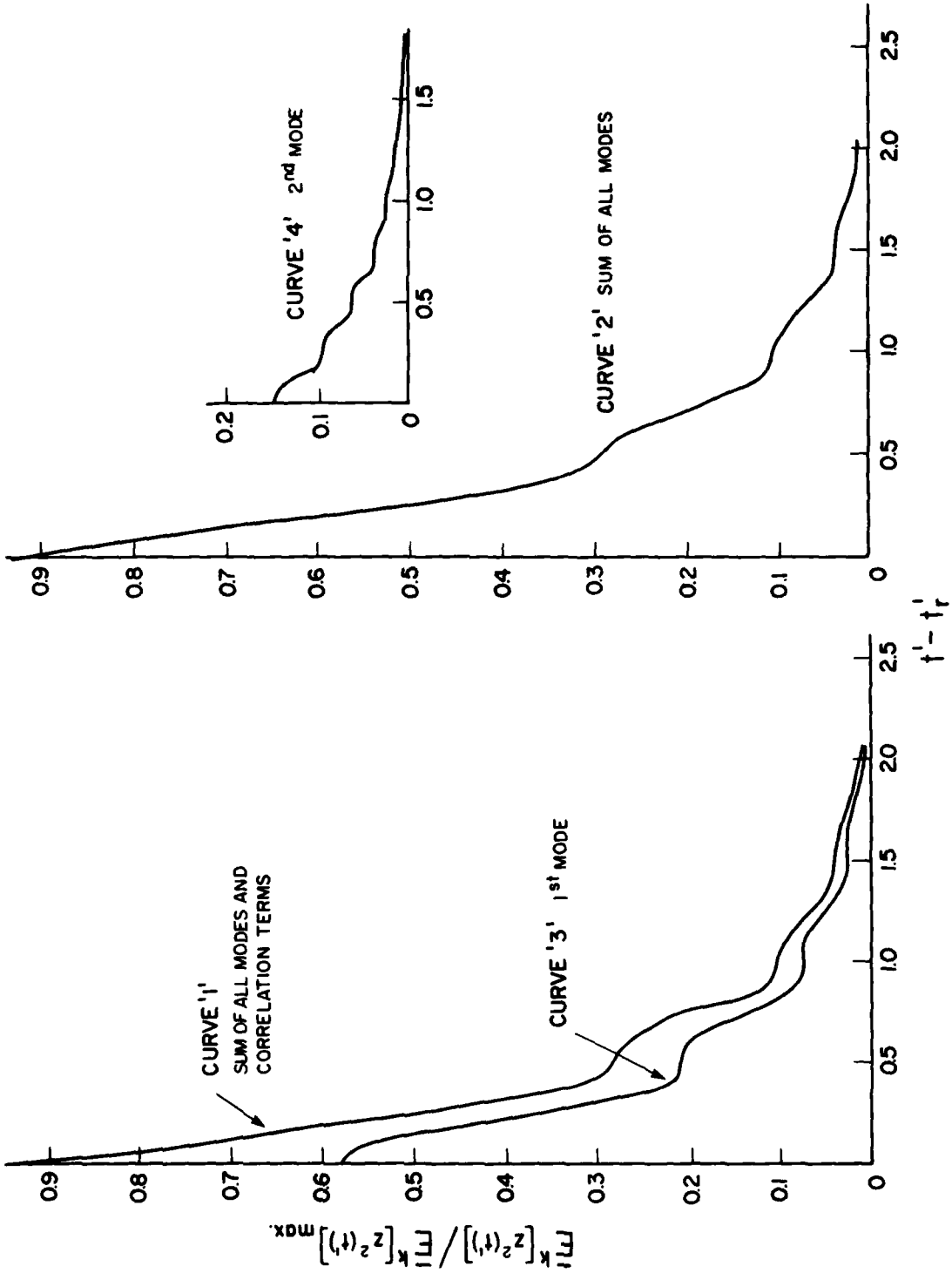

FIG. 17: DECAY TO PULSE MODULATED BUFFET LOAD AT CENTRE OF PANEL 18
FOR WHITE NOISE PRESSURE POWER SPECTRAL DENSITIES ($\Delta t' = 2.0$)

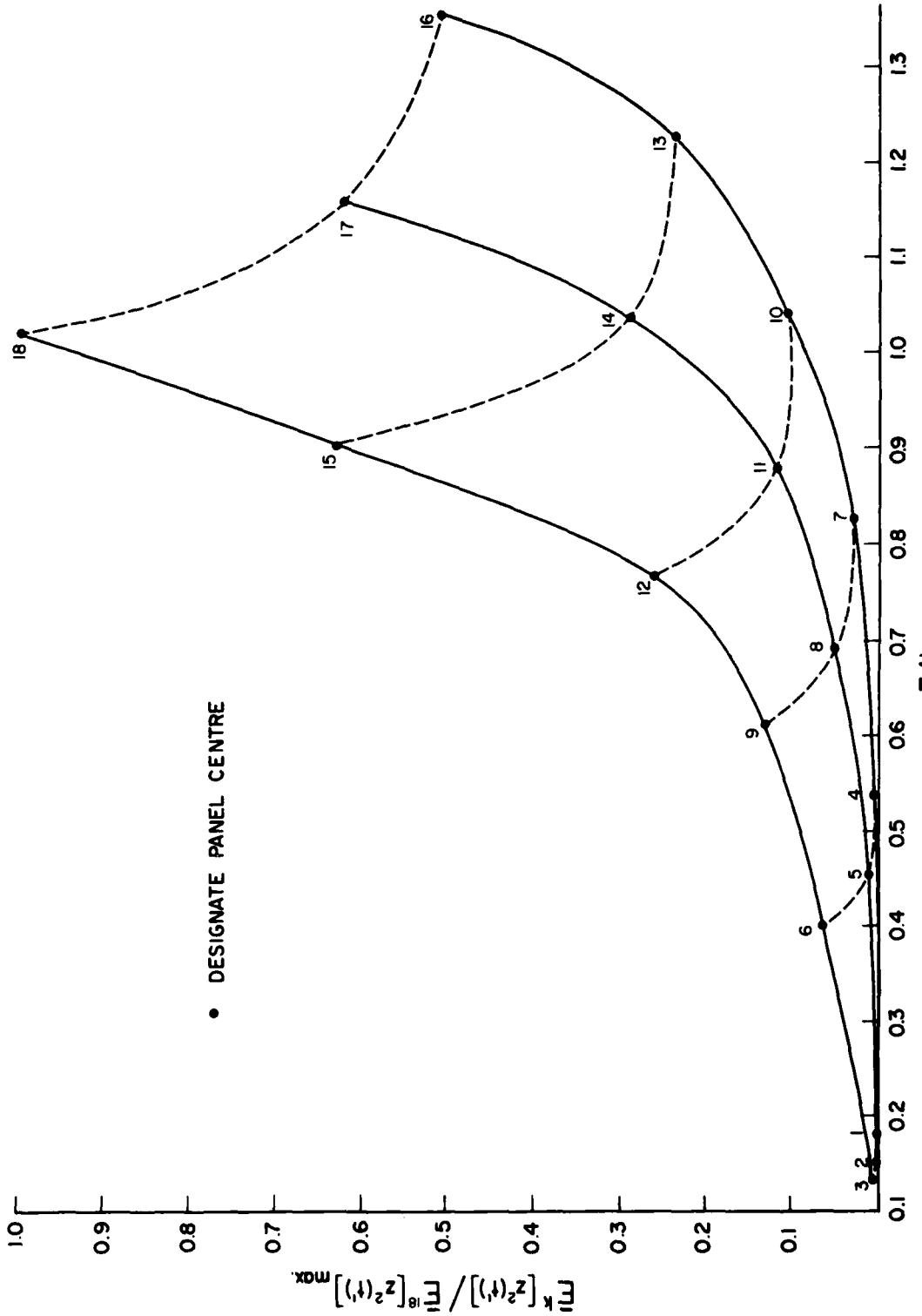

FIG. 18: MAXIMUM DISPLACEMENT RESPONSE FOR WHITE NOISE PRESSURE POWER SPECTRAL DENSITIES AT PANEL CENTRES

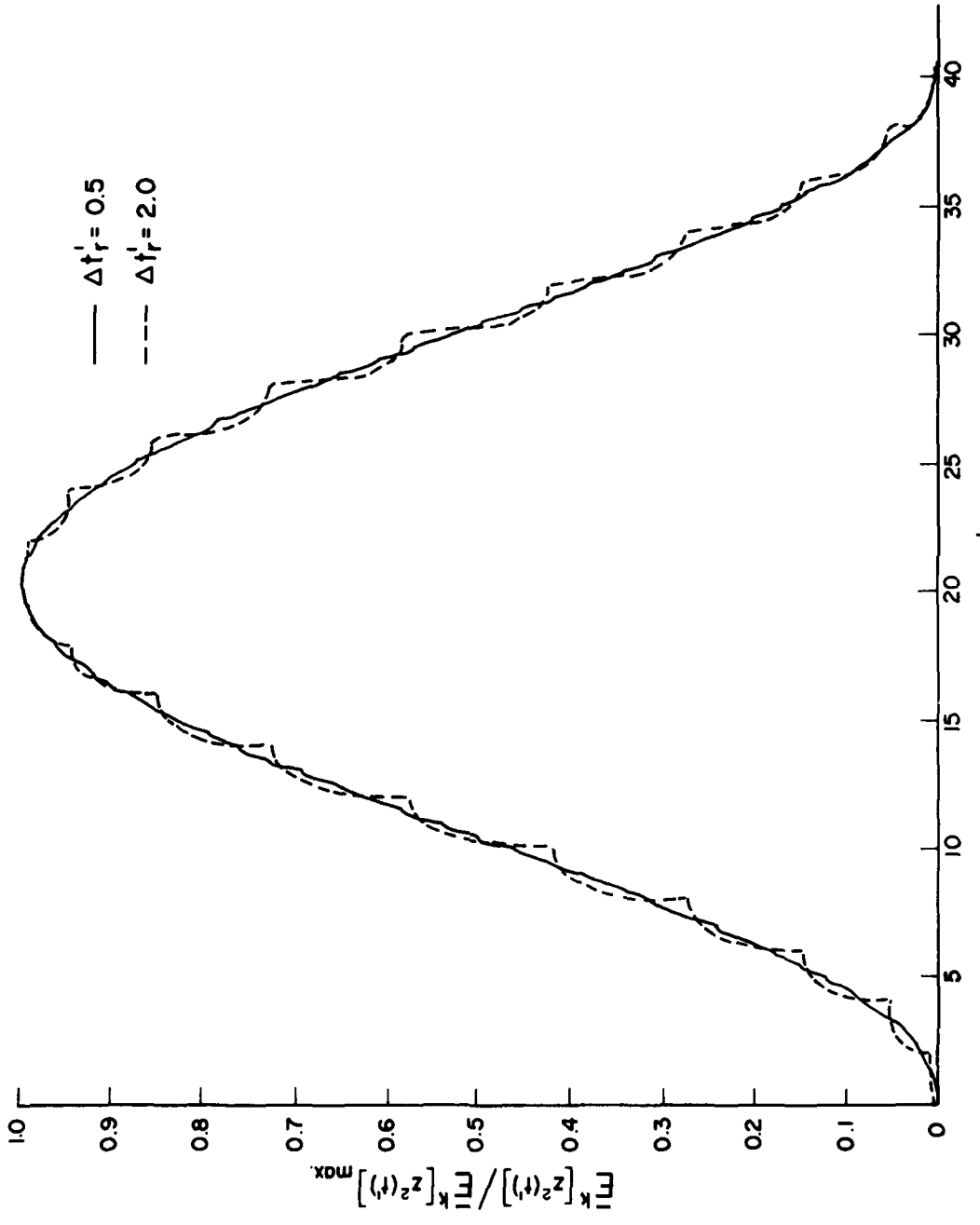

FIG. 19: MEAN SQUARE DISPLACEMENT RESPONSE AT CENTRE OF PANEL 18 FOR A SINUSOIDAL VARIATION OF ϵ WITH TIME

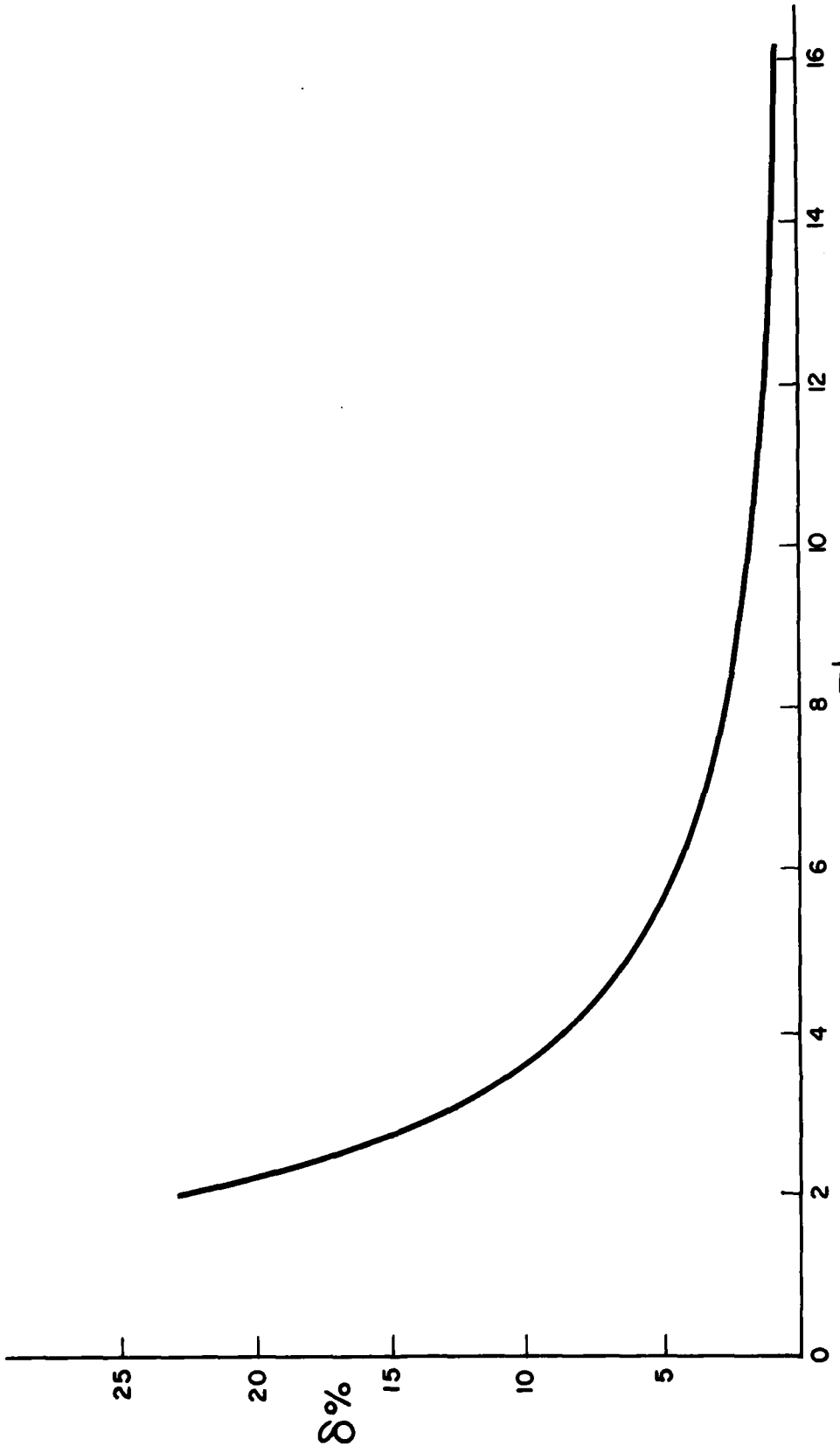

FIG. 20: AMPLITUDE DECREMENT δ VERSUS T_B' FOR PANEL 18

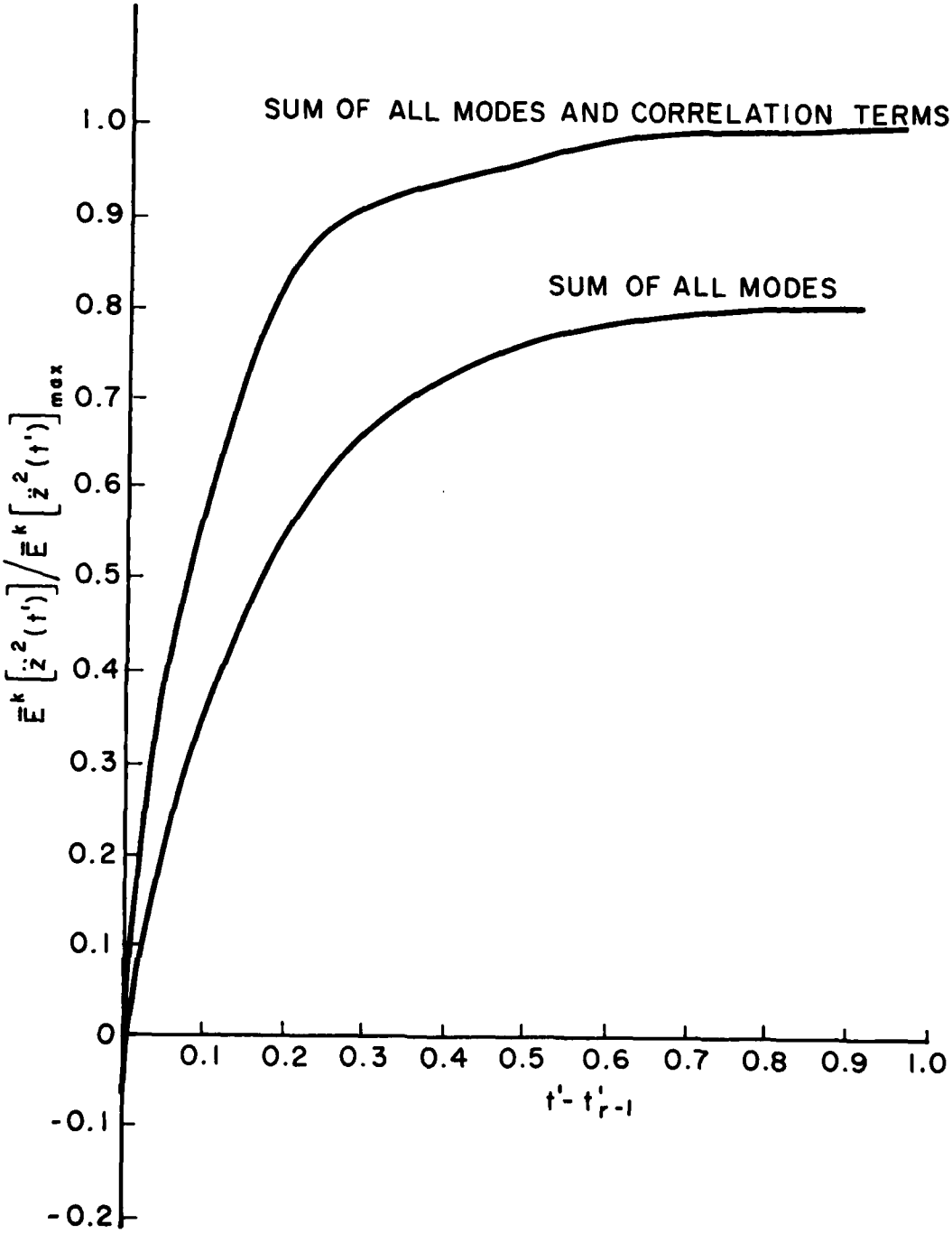

FIG. 21: ACCELERATION RESPONSE TO STEP MODULATED BUFFET LOAD AT CENTRE OF PANEL 18 FOR WHITE NOISE POWER SPECTRAL DENSITIES

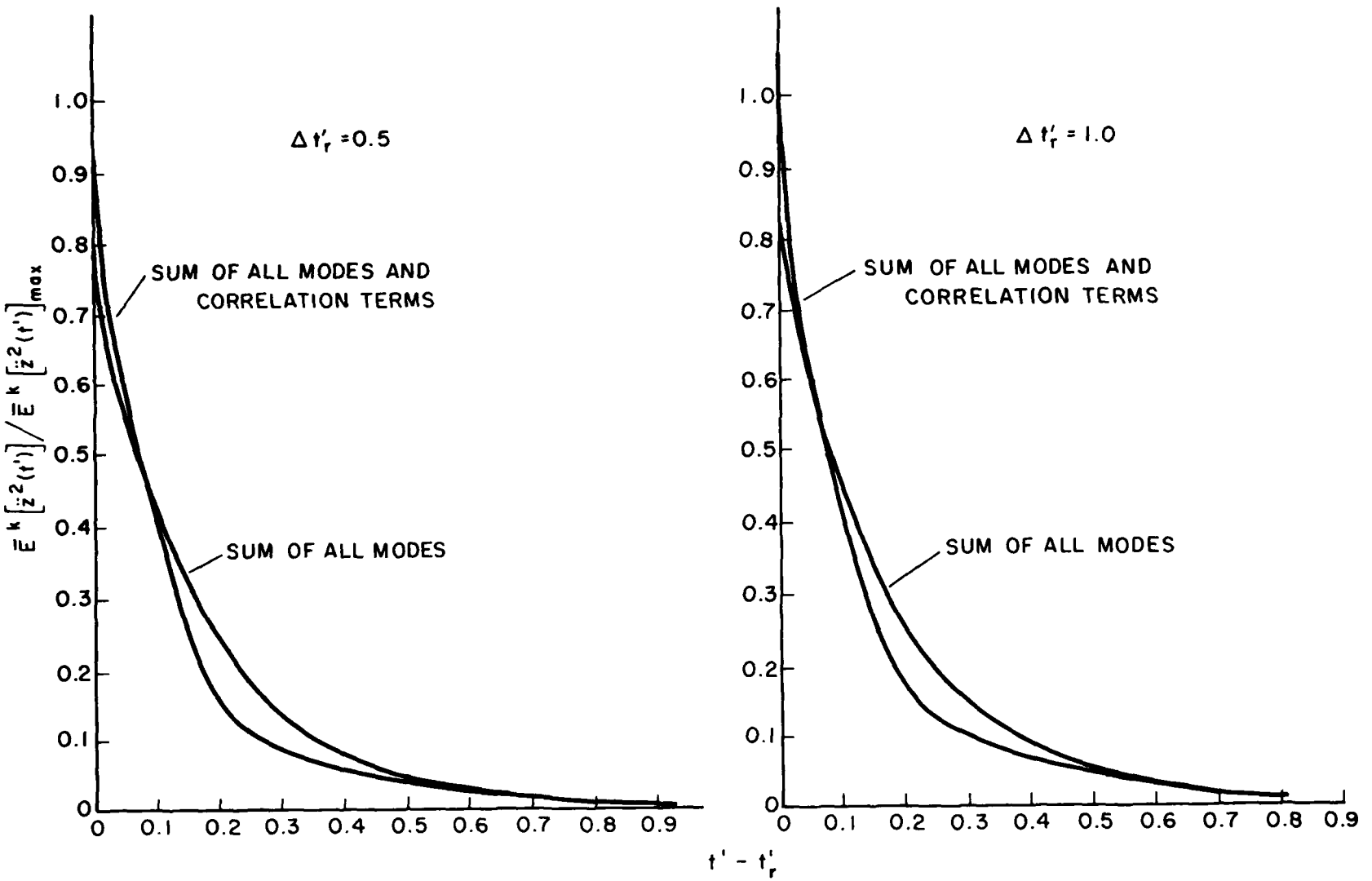

FIG. 22: DECAY TO PULSE MODULATED BUFFET LOAD AT CENTRE OF PANEL 18 FOR WHITE NOISE POWER SPECTRAL DENSITIES

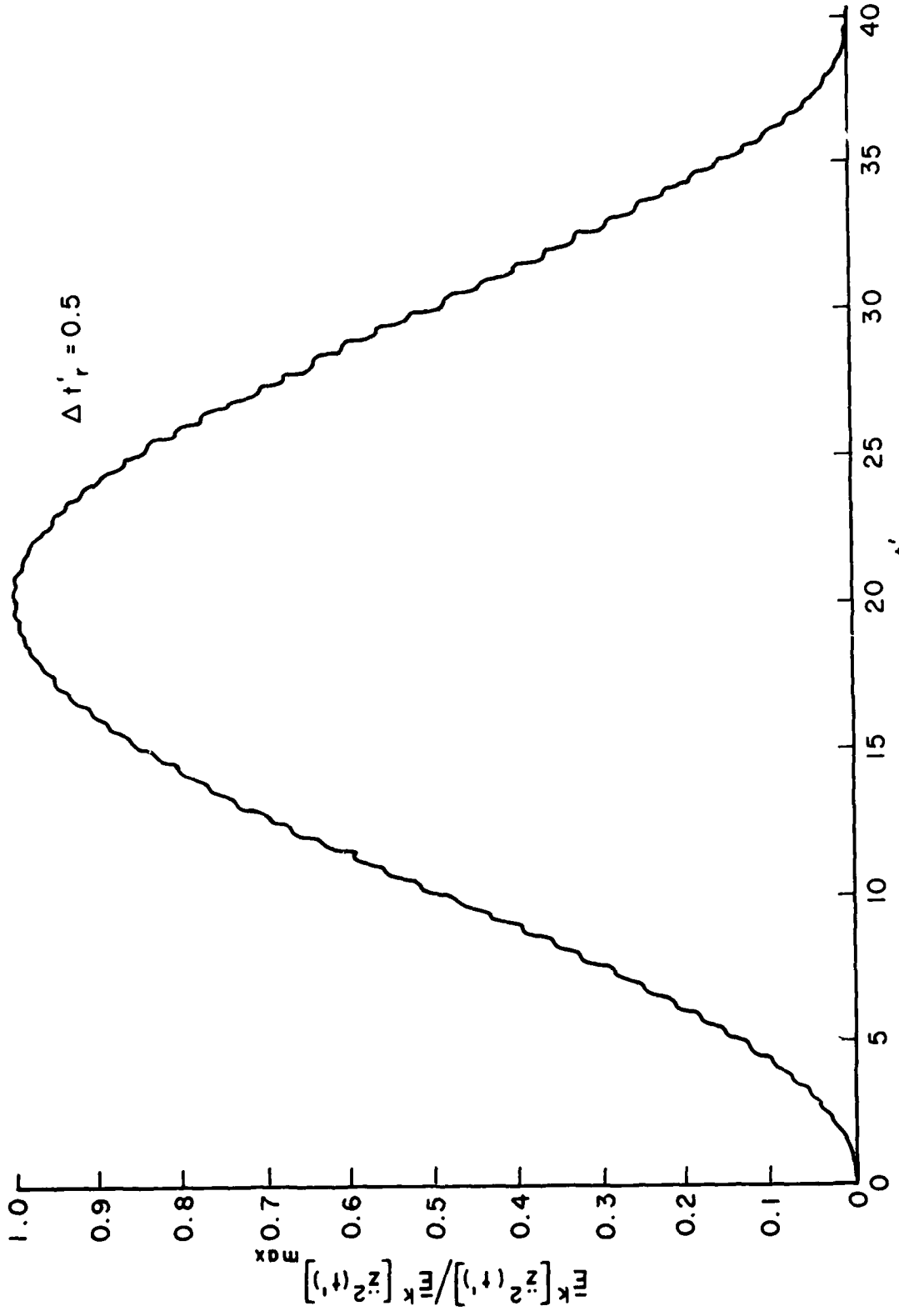

FIG. 23: MEAN SQUARE ACCELERATION RESPONSE AT CENTRE OF PANEL 18 FOR A SINUSOIDAL VARIATION OF ϵ WITH TIME

APPENDIX A

Expressions for $I_{i_r}(t_1,\omega)I^*_{j_r}(t_2,\omega)$

For $t_{r-1} \leqslant t_1 \leqslant t_r$, $t_{r-1} \leqslant t_2 \leqslant t_r$:

$$
\begin{aligned}
I_{i_r}(t_1,\omega)I^*_{j_r}(t_2,\omega) &= \epsilon_r^2 H_i(\omega)H_j^*(\omega) \\
&\cdot \Big\{ e^{i\omega(t_1-t_2)} - e^{-i\omega(t_2-t_{r-1})}\Big(\psi_i(t_1-t_{r-1}) \\
&+ i\frac{\omega}{\omega_{i_d}}\phi_i(t_1-t_{r-1})\Big) - e^{i\omega(t_1-t_{r-1})}\Big(\psi_j(t_2-t_{r-1}) \\
&- i\frac{\omega}{\omega_{j_d}}\phi_j(t_2-t_{r-1})\Big) + \psi_i(t_1-t_{r-1})\psi_j(t_2-t_{r-1}) \\
&+ \frac{\omega^2}{\omega_{i_d}\omega_{j_d}}\phi_i(t_1-t_{r-1})\phi_j(t_2-t_{r-1}) + i\frac{\omega}{\omega_{i_d}}\Big(\psi_j(t_2-t_{r-1})\phi_i(t_1-t_{r-1}) \\
&- \psi_i(t_1-t_{r-1})\phi_j(t_2-t_{r-1})\frac{\omega_{i_d}}{\omega_{j_d}}\Big)\Big\}
\end{aligned}
\tag{A1}
$$

For $t_1 \geqslant t_r$, $t_2 \geqslant t_r$:

$$
\begin{aligned}
I_{i_r}(t_1,\omega)I^*_{j_r}(t_2\omega) &= \epsilon_r^2 H_i(\omega)H_j^*(\omega) \\
&\cdot \Big\{\psi_i(t_1-t_r)\psi_j(t_2-t_r) + \frac{\omega^2}{\omega_{i_d}\omega_{j_d}}\phi_i(t_1-t_r)\phi_j(t_2-t_r) \\
&+ i\frac{\omega}{\omega_{i_d}}\phi_i(t_1-t_r)\psi_j(t_2-t_r) - i\frac{\omega}{\omega_{j_d}}\phi_j(t_2-t_r)\psi_i(t_1-t_r) \\
&+ \psi_i(t_1-t_{r-1})\psi_j(t_2-t_{r-1}) + \frac{\omega^2}{\omega_{i_d}\omega_{j_d}}\phi_i(t_1-t_{r-1})\phi_j(t_2-t_{r-1})
\end{aligned}
$$

44- Blank

$$
\left.
\begin{aligned}
&+ \; i\frac{\omega}{\omega_{i_d}}\,\phi_i(t_1-t_{r-1})\psi_j(t_2-t_{r-1}) - i\frac{\omega}{\omega_{j_d}}\,\phi_j(t_2-t_{r-1})\psi_i(t_1-t_{r-1}) \\
&- \; e^{-i\omega(t_r-t_{r-1})}\cdot\left[\psi_i(t_1-t_{r-1})\psi_j(t_2-t_r) + \frac{\omega^2}{\omega_{i_d}\omega_{j_d}}\,\phi_i(t_1-t_{r-1})\phi_j(t_2-t_r)\right. \\
&+ \; \left. i\frac{\omega}{\omega_{i_d}}\,\phi_i(t_1-t_{r-1})\psi_j(t_2-t_r) - i\frac{\omega}{\omega_{j_d}}\,\phi_j(t_2-t_r)\psi_i(t_1-t_{r-1})\right] \\
&- \; e^{i\omega(t_r-t_{r-1})}\left[\psi_i(t_1-t_r)\psi_j(t_2-t_{r-1}) + \frac{\omega^2}{\omega_{i_d}\omega_{j_d}}\,\phi_i(t_1-t_r)\phi_j(t_2-t_{r-1})\right. \\
&+ \; \left.\left. i\frac{\omega}{\omega_{i_d}}\,\phi_i(t_1-t_r)\psi_j(t_2-t_{r-1}) - \frac{i\omega}{\omega_{j_d}}\,\phi_j(t_2-t_{r-1})\psi_i(t_1-t_r)\right]\right\}
\end{aligned}
\right\} \tag{A2}
$$

where

$$\psi_i(t) = e^{-\zeta_i\omega_{i_n}t}\left(\cos\omega_{i_d}t + \zeta_i\frac{\omega_{i_n}}{\omega_{i_d}}\sin\omega_{i_d}t\right) \tag{A3}$$

$$\phi_i(t) = e^{-\zeta_i\omega_{i_n}t}\sin\omega_{i_d}t \tag{A4}$$

$$\omega_{i_d} = \sqrt{1-\zeta_i^2}\,\omega_{i_n} \tag{A5}$$

Expressions similar to Equations (A3) to (A5) are obtained for $\psi_j(t)$, $\phi_j(t)$ and ω_{j_d} by changing the subscript i in the equations to j.

APPENDIX B

Expressions for $\tilde{E}[z_{i_r}(t_1)z_{j_r}(t_2)]$

For $t_{r-1} \leqslant t_1 \leqslant t_r$, $t_{r-1} \leqslant t_2 \leqslant t_r$:

$$\tilde{E}[z_{i_r}(t_1)z_{j_r}(t_2)] = \frac{\epsilon_r^2 \pi S_r^k}{2\zeta_i \omega_{i_n}^3 M_i M_j} \cdot \Psi_a$$

$$\begin{aligned}\Psi_a = 4\zeta_i \Big\{ & \Phi_4(t_1-t_2) - \psi_i(t_1-t_{r-1})\Phi_2(t_2-t_{r-1}) - \phi_i(t_1-t_{r-1})\Phi_3(t_2-t_{r-1}) \\ & - \psi_j(t_2-t_{r-1})\Phi_4(t_1-t_{r-1}) - \phi_j(t_2-t_{r-1})\Phi_5(t_1-t_{r-1}) \\ & + \psi_i(t_1-t_{r-1})\psi_j(t_2-t_{r-1})\Phi_1 - \phi_i(t_1-t_{r-1})\phi_j(t_2-t_{r-1})\Phi_6 \\ & - \left[\psi_j(t_2-t_{r-1})\phi_i(t_1-t_{r-1}) - \psi_i(t_1-t_{r-1})\phi_j(t_2-t_{r-1})\frac{\omega_{i_d}}{\omega_{j_d}}\right]\Phi_7 \Big\}\end{aligned} \quad \text{(B1)}$$

For $t_1 \geqslant t_r$, $t_2 \geqslant t_r$:

$$\tilde{E}[z_{i_r}(t_1)z_{j_r}(t_2)] = \frac{\epsilon_r^2 \pi S_r^k}{2\zeta_i \omega_{i_n}^3 M_i M_j} \cdot \Psi_a$$

$$\begin{aligned}\Psi_a = 4\zeta_i \Big\{ & \lambda_1(t_1,t_2)\Phi_1 - \lambda_2(t_1,t_2)\Phi_6 - \left[\lambda_3(t_1,t_2) - \lambda_4(t_1,t_2)\frac{\omega_{i_d}}{\omega_{j_d}}\right]\Phi_7 \\ & - \lambda_5(t_1,t_2)\Phi_2(t_r-t_{r-1}) - \lambda_6(t_1,t_2)\Phi_8(t_r-t_{r-1}) \\ & - \left[\lambda_7(t_1,t_2) - \lambda_8(t_1,t_2)\frac{\omega_{i_d}}{\omega_{j_d}}\right]\Phi_3(t_r-t_{r-1}) - \lambda_9(t_1,t_2)\Phi_4(t_r-t_{r-1}) \\ & + \lambda_{10}(t_1,t_2)\Phi_9(t_r-t_{r-1}) + \left[\lambda_{11}(t_1,t_2)\frac{\omega_{j_d}}{\omega_{i_d}} - \lambda_{12}(t_1,t_2)\right]\Phi_5(t_r-t_{r-1}) \Big\}\end{aligned} \quad \text{(B2)}$$

where

$$\Phi_1 = \frac{d}{\frac{\omega_{i_d}}{\omega_{i_n}} \cdot D} \tag{B3}$$

$$\Phi_2(t) = \frac{e^{-\zeta_j \omega_{j_n} t}}{\frac{\omega_{j_n}}{\omega_{i_n}} D} (a \sin \omega_{j_d} t + b \cos \omega_{j_d} t) \tag{B4}$$

$$\Phi_3(t) = \frac{e^{-\zeta_j \omega_{j_n} t}}{\frac{\omega_{i_d}}{\omega_{i_n}} \frac{\omega_{j_d}}{\omega_{i_n}} D} (b_1 \sin \omega_{j_d} t - a_1 \cos \omega_{j_d} t) \tag{B5}$$

$$\Phi_4(t) = \frac{e^{-\zeta_i \omega_{i_n} t}}{\frac{\omega_{i_d}}{\omega_{i_n}} D} (d \cos \omega_{i_d} t - c \sin \omega_{i_d} t) \tag{B6}$$

$$\Phi_5(t) = \frac{e^{-\zeta_i \omega_{i_n} t}}{\frac{\omega_{i_d}}{\omega_{i_n}} \frac{\omega_{j_d}}{\omega_{i_n}} D} (e \cos \omega_{i_d} t - f \sin \omega_{i_d} t) \tag{B7}$$

$$\Phi_6 = \frac{h}{\frac{\omega_{i_d}^2}{\omega_{i_n}^2} \frac{\omega_{j_d}}{\omega_{i_n}} D} \tag{B8}$$

$$\Phi_7 = \frac{e}{\frac{\omega_{i_d}^2}{\omega_{i_n}^2} D} \tag{B9}$$

$$\Phi_8(t) = \frac{e^{-\zeta_j \omega_{j_n} t}}{\frac{\omega_{i_d}}{\omega_{i_n}} \frac{\omega_{j_d}^2}{\omega_{i_n}^2} D} (g \sin \omega_{j_d} t + j \cos \omega_{j_d} t) \quad \text{(B10)}$$

$$\Phi_9(t) = \frac{e^{-\zeta_i \omega_{i_n} t}}{\frac{\omega_{i_d}^2}{\omega_{i_n}^2} \frac{\omega_{j_d}}{\omega_{i_n}} D} (\ell \cos \omega_{i_d} t + k \sin \omega_{i_d} t) \quad \text{(B11)}$$

and

$$a = \frac{\omega_{i_d}^2}{\omega_{i_n}^2} - \frac{\omega_{j_d}^2}{\omega_{i_n}^2} + \left(\zeta_i + \zeta_j \frac{\omega_{j_n}}{\omega_{i_n}}\right)^2 \quad \text{(B12)}$$

$$b = 2 \frac{\omega_{j_d}}{\omega_{i_n}} \left(\zeta_i + \zeta_j \frac{\omega_{j_n}}{\omega_{i_n}}\right) \quad \text{(B13)}$$

$$D = a + b$$

$$a_1 = a \frac{\omega_{j_d}}{\omega_{i_n}} - b\zeta_j \frac{\omega_{j_n}}{\omega_{i_n}} \quad \text{(B14)}$$

$$b_1 = a\zeta_j \frac{\omega_{j_n}}{\omega_{i_n}} + b \frac{\omega_{j_d}}{\omega_{i_n}} \quad \text{(B15)}$$

$$c = \frac{\omega_{i_d}^2}{\omega_{i_n}^2} - \frac{\omega_{j_d}^2}{\omega_{i_n}^2} - \left(\zeta_i + \zeta_j \frac{\omega_{j_n}}{\omega_{i_n}}\right)^2 \quad \text{(B16)}$$

$$d = 2 \frac{\omega_{i_d}}{\omega_{i_n}} \left(\zeta_i + \zeta_j \frac{\omega_{j_n}}{\omega_{i_n}}\right) \quad \text{(B17)}$$

$$e = \frac{\omega_{i_d}}{\omega_{i_n}} c + \zeta_i d \tag{B18}$$

$$f = \zeta_i c - \frac{\omega_{i_d}}{\omega_{i_n}} d \tag{B19}$$

$$g = a_1 \frac{\omega_{j_d}}{\omega_{i_n}} - b_1 \zeta_j \frac{\omega_{j_n}}{\omega_{i_n}} \tag{B20}$$

$$h = \frac{\omega_{i_d}}{\omega_{i_n}} f + \zeta_i e \tag{B21}$$

$$j = a_1 \zeta_j \frac{\omega_{j_n}}{\omega_{i_n}} + b_1 \frac{\omega_{j_d}}{\omega_{i_n}} \tag{B22}$$

$$k = e \frac{\omega_{i_d}}{\omega_{i_n}} - \zeta_i f \tag{B23}$$

$$\ell = f \frac{\omega_{i_d}}{\omega_{i_n}} + \zeta_i e \tag{B24}$$

The expressions for the λ's are given by the following:

$$\lambda_1(t_1,t_2) = \psi_i(t_1-t_r)\psi_j(t_2-t_r) + \psi_i(t_1-t_{r-1})\psi_j(t_2-t_{r-1}) \tag{B25}$$

$$\lambda_2(t_1,t_2) = \phi_i(t_1-t_r)\phi_j(t_2-t_r) + \phi_i(t_1-t_{r-1})\phi_j(t_2-t_{r-1}) \tag{B26}$$

$$\lambda_3(t_1,t_2) = \phi_i(t_1-t_r)\psi_j(t_2-t_r) + \phi_i(t_1-t_{r-1})\psi_j(t_2-t_{r-1}) \tag{B27}$$

$$\lambda_4(t_1,t_2) = \phi_j(t_2-t_r)\psi_i(t_1-t_r) + \phi_j(t_2-t_{r-1})\psi_i(t_1-t_{r-1}) \quad \text{(B28)}$$

$$\lambda_5(t_1,t_2) = \psi_i(t_1-t_{r-1})\psi_j(t_2-t_r) \quad \text{(B29)}$$

$$\lambda_6(t_1,t_2) = \phi_i(t_1-t_{r-1})\phi_j(t_2-t_r) \quad \text{(B30)}$$

$$\lambda_7(t_1,t_2) = \phi_i(t_1-t_{r-1})\psi_j(t_2-t_r) \quad \text{(B31)}$$

$$\lambda_8(t_1,t_2) = \phi_j(t_2-t_r)\psi_i(t_1-t_{r-1}) \quad \text{(B32)}$$

$$\lambda_9(t_1,t_2) = \psi_i(t_1-t_r)\psi_j(t_2-t_{r-1}) \quad \text{(B33)}$$

$$\lambda_{10}(t_1,t_2) = \phi_i(t_1-t_r)\phi_j(t_2-t_{r-1}) \quad \text{(B34)}$$

$$\lambda_{11}(t_1,t_2) = \phi_i(t_1-t_r)\psi_j(t_2-t_{r-1}) \quad \text{(B35)}$$

$$\lambda_{12}(t_1,t_2) = \phi_j(t_2-t_{r-1})\psi_i(t_1-t_r) \quad \text{(B36)}$$

The expressions for ψ_i and ϕ_i are given by Equations (A3) and (A4).

APPENDIX C

Expressions for $\tilde{E}^{km}[z_{i_r}(t_1)z_{j_r}(t_2)]$

For $t_{r-1} \leqslant t_1 \leqslant t_r$, $t_{r-1} \leqslant t_2 \leqslant t_r$:

$$\tilde{E}^{km}[z_{i_r}(t_1)z_{j_r}(t_2)] = \frac{\epsilon_r^2 \pi S_r^{km}}{2\zeta_i M_i M_j \omega_{i_n}^3} \cdot \Psi_b$$

$$\Psi_b = 4\zeta_i \Bigg\{ - \Phi_4'(t_1-t_2) + \psi_i(t_1-t_{r-1})\psi_j(t_2-t_{r-1})\Phi_1'$$

$$- \frac{\omega_{i_n}}{\omega_{i_d}}\left[\psi_j(t_2-t_{r-1})\phi_i(t_1-t_{r-1}) - \psi_i(t_1-t_{r-1})\phi_j(t_2-t_{r-1})\frac{\omega_{i_d}}{\omega_{j_d}}\right]\Phi_7'$$

$$+ \phi_i(t_1-t_{r-1})\phi_j(t_2-t_{r-1})\frac{\omega_{i_n}^2}{\omega_{i_d}\omega_{j_d}}\Phi_6' - \psi_i(t_1-t_{r-1})\Phi_2'(t_2-t_{r-1})$$

$$- \phi_i(t_1-t_{r-1})\frac{\omega_{i_n}}{\omega_{i_d}}\Phi_3'(t_2-t_{r-1}) + \psi_j(t_2-t_{r-1})\Phi_4'(t_1-t_{r-1})$$

$$- \phi_j(t_2-t_{r-1})\frac{\omega_{i_n}}{\omega_{j_d}}\Phi_5'(t_1-t_{r-1})\Bigg\} \qquad \text{(C1)}$$

For $t_1 \geqslant t_r$, $t_2 \geqslant t_r$:

$$\tilde{E}^{km}[z_{i_r}(t_1)z_{j_r}(t_2)] = \frac{\epsilon_r^2 \pi S_r^{km}}{2\zeta_i M_i M_j \omega_{i_n}^3} \cdot \Psi_b$$

$$\Psi_b = 4\zeta_i \Bigg\{ \lambda_1(t_1,t_2)\Phi_1' + \lambda_2(t_1,t_2)\frac{\omega_{i_n}^2}{\omega_{i_d}\omega_{j_d}}\Phi_6' - \left[\lambda_3(t_1,t_2) - \lambda_4(t_1,t_2)\frac{\omega_{i_d}}{\omega_{j_d}}\right]\frac{\omega_{i_n}}{\omega_{i_d}}\Phi_7'$$

$$- \lambda_5(t_1,t_2)\Phi_2'(t_r-t_{r-1}) - \lambda_6(t_1,t_2)\frac{\omega_{i_n}^2}{\omega_{i_d}\omega_{j_d}}\Phi_8'(t_r-t_{r-1}) \qquad \text{(C2)}$$

52. Blank

$$
\left.
\begin{aligned}
&- \left[\lambda_7(t_1,t_2) - \lambda_8(t_1,t_2)\frac{\omega_{i_d}}{\omega_{j_d}}\right]\frac{\omega_{i_n}}{\omega_{i_d}}\,\Phi_3'(t_r - t_{r-1}) \\
&+ \lambda_9(t_1,t_2)\Phi_4'(t_r - t_{r-1}) - \lambda_{10}(t_1,t_2)\frac{\omega_{i_n}^2}{\omega_{i_d}\omega_{j_d}}\Phi_9'(t_r - t_{r-1}) \\
&+ \left[\lambda_{11}(t_1,t_2)\frac{\omega_{j_d}}{\omega_{i_d}} - \lambda_{12}(t_1,t_2)\right]\frac{\omega_{i_n}}{\omega_{j_d}}\,\Phi_5'(t_r - t_{r-1})\Big\}
\end{aligned}
\right)
$$

The λ's can be obtained from Equations (B25) to (B36), while the Φ''s are given by the following:

$$\Phi_1' = -\frac{H_2}{L_1} + \frac{\omega_{i_n}^3}{\alpha^3{}_r^{km}}\frac{I_1}{L_2} \tag{C3}$$

$$
\begin{aligned}
\Phi_2'(t) = {} & e^{-\zeta_j \omega_{j_n} t}\cdot\frac{1}{E_1}(-A_1 \sin\omega_{j_d} t + A_2 \cos\omega_{j_d} t) \\
& + \frac{\omega_{i_n}^3}{\alpha^3{}_r^{km}}\, e^{-\alpha_r^{km} t}\cdot\frac{1}{E_2}\left(B_1 \cos\beta_r^{km} t - \frac{\omega_{i_n}}{\alpha_r^{km}} B_2 \sin\beta_r^{km} t\right)
\end{aligned} \tag{C4}
$$

$$
\begin{aligned}
\Phi_3'(t) = {} & e^{-\zeta_j \omega_{j_n} t}\cdot\frac{1}{E_1}(F_1 \cos\omega_{j_d} t + F_2 \sin\omega_{j_d} t) \\
& + e^{-\alpha_r^{km} t}\cdot\frac{\omega_{i_n}^2}{\alpha^2{}_r^{km}}\cdot\frac{1}{E_2}(G_1 \sin\beta_r^{km} t + G_2 \cos\beta_r^{km} t)
\end{aligned} \tag{C5}
$$

$$
\begin{aligned}
\Phi_4'(t) = {} & e^{-\zeta_i \omega_{i_n} t}\cdot\frac{1}{L_1}(H_1 \sin\omega_{i_d} t + H_2 \cos\omega_{i_d} t) \\
& - e^{-\alpha_r^{km} t}\cdot\frac{\omega_{i_n}^3}{\alpha^3{}_r^{km}}\cdot\frac{1}{L_2}\left(I_1 \cos\beta_r^{km} t - \frac{\omega_{i_n}}{\alpha_r^{km}} I_2 \sin\beta_r^{km} t\right)
\end{aligned} \tag{C6}
$$

$$\Phi_5'(t) = e^{-\zeta_i \omega_{i_n} t} \cdot \frac{1}{L_1} (J_1 \cos \omega_{i_d} t - J_2 \sin \omega_{i_d} t) + e^{-\alpha_r^{km} t} \cdot \frac{\omega_{i_n}^2}{\alpha_r^{2\,km}} \frac{1}{L_2} (K_1 \sin \beta_r^{km} t + K_2 \cos \beta_r^{km} t) \quad \text{(C7)}$$

$$\Phi_6' = -\frac{M_2}{L_1} + \frac{\omega_{i_n}}{\alpha_r^{km}} \frac{N_1}{L_2} \quad \text{(C8)}$$

$$\Phi_7' = \frac{J_1}{L_1} + \frac{\omega_{i_n}^2}{\alpha_r^{2\,km}} \frac{K_2}{L_2} \quad \text{(C9)}$$

$$\Phi_8'(t) = e^{-\zeta_j \omega_{j_n} t} \cdot \frac{1}{E_1} (Q_2 \cos \omega_{j_d} t - Q_1 \sin \omega_{j_d} t) + e^{-\alpha_r^{km} t} \cdot \frac{\omega_{i_n}}{\alpha_r^{km}} \frac{1}{E_2} (R_1 \cos \beta_r^{km} t - R_2 \sin \beta_r^{km} t) \quad \text{(C10)}$$

$$\Phi_9'(t) = -e^{-\zeta_i \omega_{i_n} t} \cdot \frac{1}{L_1} (M_1 \sin \omega_{i_d} t + M_2 \cos \omega_{i_d} t) + e^{-\alpha_r^{km} t} \cdot \frac{\omega_{i_n}}{\alpha_r^{km}} \frac{1}{L_2} (N_1 \cos \beta_r^{km} t - N_2 \sin \beta_r^{km} t) \quad \text{(C11)}$$

where

$$A_1 = \left(a_2^2 - b_1 b_2 \frac{\omega_{i_n}^2}{\alpha_r^{2\,km}}\right)(a_1 \gamma_2 + cx) - \frac{\omega_{i_n}}{\alpha_r^{km}} a_2 (b_1 + b_2)(c\gamma_2 - a_1 x) \quad \text{(C12)}$$

$$A_2 = \left(a_2^2 - b_1 b_2 \frac{\omega_{i_n}^2}{\alpha_r^{2\,km}}\right)(c\gamma_2 - a_1 x) + \frac{\omega_{i_n}}{\alpha_r^{km}} a_2 (b_1 + b_2)(a_1 \gamma_2 + cx) \quad \text{(C13)}$$

$$B_1 = d_1 d_2 + \frac{\omega_{i_n}^2}{\alpha_r^{2\,km}} e_1 e_2 \quad \text{(C14)}$$

$$B_2 = e_2 d_1 - e_1 d_2 \tag{C15}$$

$$E_1 = \frac{\omega_{j_d}}{\omega_{i_n}} (a_1^2 + c^2)\left(a_2^2 + \frac{\omega_{i_n}^2}{\alpha^2{}_r^{km}} b_2^2\right)\left(a_2^2 + \frac{\omega_{i_n}^2}{\alpha^2{}_r^{km}} b_1^2\right) \tag{C16}$$

$$E_2 = 2\left(d_1^2 + \frac{\omega_{i_n}^2}{\alpha^2{}_r^{km}} e_1^2\right)\left(d_2^2 + \frac{\omega_{i_n}^2}{\alpha^2{}_r^{km}} e_2^2\right) \tag{C17}$$

$$F_1 = A_1 \frac{\omega_{j_d}}{\omega_{i_n}} + A_2 \zeta_j \frac{\omega_{j_n}}{\omega_{i_n}} \tag{C18}$$

$$F_2 = A_2 \frac{\omega_{j_d}}{\omega_{i_n}} - A_1 \zeta_j \frac{\omega_{j_n}}{\omega_{i_n}} \tag{C19}$$

$$G_1 = B_1 \frac{\beta_r^{km}}{\alpha_r^{km}} - B_2 \frac{\omega_{i_n}}{\alpha_r^{km}} \tag{C20}$$

$$G_2 = B_2 \frac{\beta_r^{km}}{\alpha_r^{km}} \frac{\omega_{i_n}}{\alpha_r^{km}} + B_1 \tag{C21}$$

$$\begin{aligned} H_1 = {} & \left(\theta^2 - \frac{\omega_{i_n}^2}{\alpha^2{}_r^{km}} \mu_1 \mu_2\right)\left(2\zeta_i \frac{\omega_{i_n}}{\alpha_r^{km}} \frac{\omega_{i_d}}{\alpha_r^{km}} \delta_2 + \gamma_1 \delta_1\right) \\ & + \frac{\omega_{i_n}}{\alpha_r^{km}} \theta(\mu_1 + \mu_2)\left(2\zeta_i \frac{\omega_{i_n}}{\alpha_r^{km}} \frac{\omega_{i_d}}{\alpha_r^{km}} \delta_1 - \gamma_1 \delta_2\right) \end{aligned} \tag{C22}$$

$$\begin{aligned} H_2 = {} & \left(\theta^2 - \frac{\omega_{i_n}^2}{\alpha^2{}_r^{km}} \mu_1 \mu_2\right)\left(2\zeta_i \frac{\omega_{i_n}}{\alpha_r^{km}} \frac{\omega_{i_d}}{\alpha_r^{km}} \delta_1 - \gamma_1 \delta_2\right) \\ & - \frac{\omega_{i_n}}{\alpha_r^{km}} \theta(\mu_1 + \mu_2)\left(2\zeta_i \frac{\omega_{i_n}}{\alpha_r^{km}} \frac{\omega_{i_d}}{\alpha_r^{km}} \delta_2 + \gamma_1 \delta_1\right) \end{aligned} \tag{C23}$$

$$I_1 = \epsilon_1 \chi_1 + \frac{\omega_{i_n}^2}{\alpha_r^{2\,km}} \epsilon_2 \chi_2 \tag{C24}$$

$$I_2 = \epsilon_2 \chi_1 - \epsilon_1 \chi_2 \tag{C25}$$

$$J_1 = H_1 \frac{\omega_{i_d}}{\omega_{i_n}} - H_2 \zeta_i \tag{C26}$$

$$J_2 = H_2 \frac{\omega_{i_d}}{\omega_{i_n}} + H_1 \zeta_i \tag{C27}$$

$$K_1 = I_1 \frac{\beta_r^{km}}{\alpha_r^{km}} - I_2 \frac{\omega_{i_n}}{\alpha_r^{km}} \tag{C28}$$

$$K_2 = I_2 \frac{\omega_{i_n}}{\alpha_r^{km}} \frac{\beta_r^{km}}{\alpha_r^{km}} + I_1 \tag{C29}$$

$$L_1 = \frac{\omega_{i_d}}{\omega_{i_n}} (\delta_1^2 + \delta_2^2) \left(\theta^2 + \frac{\omega_{i_n}^2}{\alpha_r^{2\,km}} \mu_1^2 \right) \left(\theta^2 + \frac{\omega_{i_n}^2}{\alpha_r^{2\,km}} \mu_2^2 \right) \tag{C30}$$

$$L_2 = 2 \left(\epsilon_1^2 + \frac{\omega_{i_n}^2}{\alpha_r^{2\,km}} \epsilon_2^2 \right) \left(\chi_1^2 + \frac{\omega_{i_n}^2}{\alpha_r^{2\,km}} \chi_2^2 \right) \tag{C31}$$

$$M_1 = H_1 \left(\frac{\omega_{i_d}^2}{\omega_{i_n}^2} - \zeta_1^2 \right) - 2\zeta_i \frac{\omega_{i_d}}{\omega_{i_n}} H_2 \tag{C32}$$

$$M_2 = H_2 \left(\frac{\omega_{i_d}^2}{\omega_{i_n}^2} - \zeta_1^2 \right) + 2\zeta_i \frac{\omega_{i_d}}{\omega_{i_n}} H_1 \tag{C33}$$

$$N_1 = I_1\left(\frac{\beta^{2^{km}}_r}{\alpha^{2^{km}}_r} - 1\right) - 2I_2 \frac{\beta_r^{km}}{\alpha_r^{km}} \frac{\omega_{i_n}}{\alpha_r^{km}} \tag{C34}$$

$$N_2 = I_2 \frac{\omega_{i_n}}{\alpha_r^{km}}\left(\frac{\beta^{2^{km}}_r}{\alpha^{2^{km}}_r} - 1\right) + 2I_1 \frac{\beta_r^{km}}{\alpha_r^{km}} \tag{C35}$$

$$Q_1 = A_1\left(\frac{\omega_{j_d}^2}{\omega_{i_n}^2} - \zeta_j^2 \frac{\omega_{j_n}^2}{\omega_{i_n}^2}\right) + 2A_2\zeta_j \frac{\omega_{j_n}}{\omega_{i_n}} \frac{\omega_{j_d}}{\omega_{i_n}} \tag{C36}$$

$$Q_2 = A_2\left(\frac{\omega_{j_d}^2}{\omega_{i_n}^2} - \zeta_j^2 \frac{\omega_{j_n}^2}{\omega_{i_n}^2}\right) - 2A_1\zeta_j \frac{\omega_{j_n}}{\omega_{i_n}} \frac{\omega_{j_d}}{\omega_{i_n}} \tag{C37}$$

$$R_1 = B_1\left(\frac{\beta^{2^{km}}_r}{\alpha^{2^{km}}_r} - 1\right) - 2B_2 \frac{\beta_r^{km}}{\alpha_r^{km}} \frac{\omega_{i_n}}{\alpha_r^{km}} \tag{C38}$$

$$R_2 = B_2 \frac{\omega_{i_n}}{\alpha_r^{km}}\left(\frac{\beta^{2^{km}}_r}{\alpha^{2^{km}}_r} - 1\right) + 2B_1 \frac{\beta_r^{km}}{\alpha_r^{km}} \tag{C39}$$

$$a_1 = \frac{\omega_{j_d}^2}{\omega_{i_n}^2} - \frac{\omega_{i_d}^2}{\omega_{i_n}^2} - \left(\zeta_i + \zeta_j \frac{\omega_{j_n}}{\omega_{i_n}}\right)^2 \tag{C40}$$

$$a_2 = \frac{\omega_{j_d}^2}{\alpha^{2^{km}}_r} - \frac{\beta^{2^{km}}_r}{\alpha^{2^{km}}_r} + 1 - \zeta_j^2 \frac{\omega_{j_n}^2}{\alpha^{2^{km}}_r} \tag{C41}$$

$$b_1 = 2\left(\zeta_j \frac{\omega_{j_n}}{\omega_{i_n}} \frac{\omega_{j_d}}{\alpha_r^{km}} - \frac{\beta_r^{km}}{\omega_{i_n}}\right) \tag{C42}$$

$$b_2 = 2\left(\zeta_j \frac{\omega_{j_n}}{\omega_{i_n}} \frac{\omega_{j_d}}{\alpha_r^{km}} + \frac{\beta_r^{km}}{\omega_{i_n}}\right) \tag{C43}$$

$$c = 2\frac{\omega_{j_d}}{\omega_{i_n}}\left(\zeta_i + \zeta_j \frac{\omega_{j_n}}{\omega_{i_n}}\right) \tag{C44}$$

$$d_1 = -\frac{\omega_{i_d}^2}{\alpha_r^{2\,km}} + \frac{\beta_r^{2\,km}}{\alpha_r^{2\,km}} - \left(\zeta_i \frac{\omega_{i_n}}{\alpha_r^{km}} + 1\right)^2 \tag{C45}$$

$$d_2 = -\frac{\omega_{j_d}^2}{\alpha_r^{2\,km}} + \frac{\beta_r^{2\,km}}{\alpha_r^{2\,km}} - \left(\zeta_j \frac{\omega_{j_n}}{\alpha_r^{km}} - 1\right)^2 \tag{C46}$$

$$e_1 = 2\frac{\beta_r^{km}}{\omega_{i_n}}\left(\zeta_i \frac{\omega_{i_n}}{\alpha_r^{km}} + 1\right) \tag{C47}$$

$$e_2 = 2\frac{\beta_r^{km}}{\omega_{i_n}}\left(\zeta_j \frac{\omega_{j_n}}{\alpha_r^{km}} - 1\right) \tag{C48}$$

$$x = 2\zeta_j \frac{\omega_{j_n}}{\alpha_r^{km}} \frac{\omega_{j_d}}{\alpha_r^{km}} \tag{C49}$$

$$\gamma_1 = \frac{\omega_{i_d}^2}{\alpha_r^{2\,km}} + \frac{\beta_r^{2\,km}}{\alpha_r^{2\,km}} + 1 - \zeta_i^2 \frac{\omega_{i_n}^2}{\alpha_r^{2\,km}} \tag{C50}$$

$$\gamma_2 = \frac{\omega_{j_d}^2}{\alpha_r^{2\,km}} + \frac{\beta_r^{2\,km}}{\alpha_r^{2\,km}} + 1 - \zeta_j^2 \frac{\omega_{j_n}^2}{\alpha_r^{2\,km}} \tag{C51}$$

$$\delta_1 = \frac{\omega_{i_d}^2}{\omega_{i_n}^2} - \frac{\omega_{j_d}^2}{\omega_{i_n}^2} - \left(\zeta_i + \frac{\omega_{j_n}}{\omega_{i_n}} \zeta_j\right)^2 \tag{C52}$$

$$\delta_2 = 2\frac{\omega_{i_d}}{\omega_{i_n}}\left(\zeta_i + \frac{\omega_{j_n}}{\omega_{i_n}} \zeta_j\right) \tag{C53}$$

$$\epsilon_1 = -\frac{\omega_{i_d}^2}{\alpha_r^{2\,km}} + \frac{\beta_r^{2\,km}}{\alpha_r^{2\,km}} - \left(\zeta_i \frac{\omega_{i_n}}{\alpha_r^{km}} - 1\right)^2 \tag{C54}$$

$$\epsilon_2 = 2\frac{\beta_r^{km}}{\omega_{i_n}}\left(\zeta_i \frac{\omega_{i_n}}{\alpha_r^{km}} - 1\right) \tag{C55}$$

$$\theta = \frac{\omega_{i_d}^2}{\alpha_r^{2\,km}} - \frac{\beta_r^{2\,km}}{\alpha_r^{2\,km}} - \zeta_i^2 \frac{\omega_{i_n}^2}{\alpha_r^{2\,km}} + 1 \tag{C56}$$

$$\mu_1 = 2\left(\zeta_i \frac{\omega_{i_d}}{\alpha_r^{km}} - \frac{\beta_r^{km}}{\omega_{i_n}}\right) \tag{C57}$$

$$\mu_2 = 2\left(\zeta_i \frac{\omega_{i_d}}{\alpha_r^{km}} + \frac{\beta_r^{km}}{\omega_{i_n}}\right) \tag{C58}$$

$$\chi_1 = -\frac{\omega_{j_d}^2}{\alpha_r^{2\,km}} + \frac{\beta_r^{2\,km}}{\alpha_r^{2\,km}} - \left(\zeta_j \frac{\omega_{j_n}}{\alpha_r^{km}} + 1\right)^2 \tag{C59}$$

$$\chi_2 = 2\frac{\beta_r^{km}}{\omega_{i_n}}\left(\zeta_j \frac{\omega_{j_n}}{\alpha_r^{km}} + 1\right) \tag{C60}$$

APPENDIX D

Expressions for $\tilde{E}[\ddot{z}_{i_r}(t)\ddot{z}_{j_r}(t)]$

For $t_{r-1} \leq t \leq t_r$:

$$\tilde{E}[\ddot{z}_{i_r}(t)\ddot{z}_{j_r}(t)] = \frac{\epsilon_r^2 \pi S_r^k \omega_{i_n}}{2\zeta_i M_i M_j} \cdot \Psi_c$$

$$\begin{aligned}
\Psi_c = 4\zeta_i \Bigg\{ & \Phi_{10} + \frac{\omega_{j_n}^2}{\omega_{i_n}^2} \Big[A_i(t-t_{r-1}) A_j(t-t_{r-1}) \Phi_1 - B_i(t-t_{r-1}) B_j(t-t_{r-1}) \Phi_6 \\
& - \left(A_j(t-t_{r-1}) B_i(t-t_{r-1}) - A_i(t-t_{r-1}) B_j(t-t_{r-1}) \frac{\omega_{i_d}}{\omega_{j_d}} \right) \Phi_7 \\
& - (1-2\zeta_j^2) \left(A_i(t-t_{r-1}) \Phi_2(t-t_{r-1}) + B_i(t-t_{r-1}) \Phi_3(t-t_{r-1}) \right) \\
& - 2\zeta_j \frac{\omega_{j_d}}{\omega_{j_n}} \left(A_i(t-t_{r-1}) \Phi_{11}(t-t_{r-1}) + B_i(t-t_{r-1}) \Phi_{12}(t-t_{r-1}) \right) \\
& - (1-2\zeta_i^2) \left(A_j(t-t_{r-1}) \Phi_4(t-t_{r-1}) + B_j(t-t_{r-1}) \Phi_5(t-t_{r-1}) \right) \\
& + 2\zeta_j \frac{\omega_{i_d}}{\omega_{i_n}} \left(A_j(t-t_{r-1}) \Phi_{13}(t-t_{r-1}) + B_j(t-t_{r-1}) \Phi_{14}(t-t_{r-1}) \right) \Big] \Bigg\}
\end{aligned} \tag{D1}$$

For $t \geq t_r$:

$$\tilde{E}[\ddot{z}_{i_r}(t)\ddot{z}_{j_r}(t)] = \frac{\epsilon_r^2 \pi S_r^k \omega_{i_n}}{2\zeta_i M_i M_j} \cdot \Psi_c$$

$$\begin{aligned}
\Psi_c = 4\frac{\omega_{j_n}^2}{\omega_{i_n}^2}\Bigg\{ & \Big(A_i(t-t_r)A_j(t-t_r) + A_i(t-t_{r-1})A_j(t-t_{r-1})\Big)\Phi_1 \\
& - \Big(B_i(t-t_r)B_j(t-t_r) + B_i(t-t_{r-1})B_j(t-t_{r-1})\Big)\Phi_6 \\
& - \Big[B_i(t-t_r)A_j(t-t_r) + B_i(t-t_{r-1})A_j(t-t_{r-1}) \\
& - \frac{\omega_{i_d}}{\omega_{j_d}}\Big(B_j(t-t_r)A_i(t-t_r) + B_j(t-t_{r-1})A_i(t-t_{r-1})\Big)\Big]\Phi_7 \\
& - A_i(t-t_{r-1})A_j(t-t_r)\Phi_2(t_r-t_{r-1}) - B_i(t-t_{r-1})B_j(t-t_r)\Phi_8(t_r-t_{r-1}) \\
& - \Big[B_i(t-t_{r-1})A_j(t-t_r) - B_j(t-t_r)A_i(t-t_{r-1})\frac{\omega_{i_d}}{\omega_{j_d}}\Big]\Phi_3(t_r-t_{r-1}) \\
& - A_i(t-t_r)A_j(t-t_{r-1})\Phi_4(t_r-t_{r-1}) + B_i(t-t_r)B_j(t-t_{r-1})\Phi_9(t_r-t_{r-1}) \\
& + \Big[B_i(t-t_r)A_j(t-t_{r-1})\frac{\omega_{j_d}}{\omega_{i_d}} - B_j(t-t_{r-1})A_i(t-t_r)\Big]\Phi_5(t_r-t_{r-1})\Bigg\}
\end{aligned} \qquad \text{(D2)}$$

where $\Phi_1, \Phi_2 \ldots . \Phi_9$ are given in Equations (B3) to (B11) of Appendix B. The expressions for Φ_{10} to Φ_{14} are:

$$\Phi_{10} = \frac{1}{\frac{\omega_{i_d}}{\omega_{i_n}} D}\left\{d\left[\left(\frac{\omega_{i_d}^2}{\omega_{i_n}^2} - \zeta_i^2\right)^2 - 4\zeta_i^2\frac{\omega_{i_d}^2}{\omega_{i_n}^2}\right] + 4\zeta_i\frac{\omega_{i_d}}{\omega_{i_n}} c\,(2\zeta_i^2 - 1)\right\} \qquad \text{(D3)}$$

$$\Phi_{11}(t) = \frac{e^{-\zeta_j \omega_{j_n} t}}{\frac{\omega_{j_d}}{\omega_{i_d}} D} \quad (a \cos \omega_{j_d} t - b \sin \omega_{j_d} t) \tag{D4}$$

$$\Phi_{12}(t) = \frac{e^{-\zeta_j \omega_{j_n} t}}{\frac{\omega_{i_d}}{\omega_{i_n}} \frac{\omega_{j_d}}{\omega_{i_n}} D} \quad (b \cos \omega_{j_d} t + a \sin \omega_{j_d} t) \tag{D5}$$

$$\Phi_{13}(t) = \frac{e^{-\zeta_i \omega_{i_n} t}}{\frac{\omega_{i_d}}{\omega_{i_n}} D} \quad (d \sin \omega_{i_d} t + c \cos \omega_{i_d} t) \tag{D6}$$

$$\Phi_{14} = \frac{e^{-\zeta_i \omega_{i_n} t}}{\frac{\omega_{i_d}}{\omega_{i_n}} \frac{\omega_{j_d}}{\omega_{i_n}} D} \quad (e \sin \omega_{i_d} t + f \cos \omega_{i_d} t) \tag{D7}$$

The relations for a, b, c, d, e, f and D are given in Appendix B. $A_i(t)$, $B_i(t)$ are obtained by differentiating $\psi_i(t)$ and $\phi_i(t)$ given by Equations (A4) and (A5) respectively. They can be written as:

$$A_i(t) = \psi_i(t) - 2\zeta_i \frac{\omega_{i_n}}{\omega_{i_d}} \phi_i(t) \tag{D8}$$

and

$$B_i(t) = 2\zeta_i \frac{\omega_{i_d}}{\omega_{i_n}} \psi_i(t) + (1 - 4\zeta_i^2)\phi_i(t) \tag{D9}$$

with similar expressions for $A_j(t)$ and $B_j(t)$.

APPENDIX E

Expressions for $\tilde{E}^{km}[\ddot{z}_{i_r}(t)\ddot{z}_{j_r}(t)]$

For $t_{r-1} \leq t \leq t_r$:

$$\tilde{E}^{km}[\ddot{z}_{i_r}(t)\ddot{z}_{j_r}(t)] = \frac{\epsilon_r^2 \pi S_r^{km} \alpha_r^{km}}{2\zeta_i M_i M_j} \cdot \Psi_d$$

$$\begin{aligned}
\Psi_d = 4\zeta_i \Bigg\{ & \Phi_{10}' - \frac{\omega_{i_n}}{\alpha_r^{km}} A_i(t-t_{r-1})\Phi_8'(t-t_{r-1}) - \frac{\omega_{i_n}^2}{\omega_{i_d}\alpha_r^{km}} B_i(t-t_{r-1})\Phi_{11}'(t-t_{r-1}) \\
& - \frac{\omega_{j_n}^2}{\omega_{i_n}\alpha_r^{km}} A_j(t-t_{r-1})\Phi_9'(t-t_{r-1}) - \frac{\omega_{j_n}^2}{\omega_{j_d}\alpha_r^{km}} B_j(t-t_{r-1})\Phi_{12}'(t-t_{r-1}) \\
& + \frac{\omega_{j_n}^2}{\omega_{i_n}\alpha_r^{km}} A_i(t-t_{r-1})A_j(t-t_{r-1})\Phi_1' \\
& + \frac{\omega_{i_n}\omega_{j_n}^2}{\omega_{i_d}\omega_{j_d}\alpha_r^{km}} B_i(t-t_{r-1})B_j(t-t_{r-1})\Phi_6' \\
& - \frac{\omega_{j_n}^2}{\omega_{i_d}\alpha_r^{km}} \left[A_j(t-t_{r-1})B_i(t-t_{r-1}) - A_i(t-t_{r-1})B_j(t-t_{r-1})\frac{\omega_{i_d}}{\omega_{j_d}} \right] \Phi_7' \Bigg\}
\end{aligned} \qquad \text{(E1)}$$

14-Blank

For $t \geqslant t_r$:

$$\tilde{E}^{km}[\ddot{z}_{i_r}(t)\ddot{z}_{j_r}(t)] = \frac{\epsilon_r^2 \pi S_r^{km} \alpha_r^{km}}{2\zeta_i M_i M_j} \cdot \Psi_d$$

$$\Psi_d = 4\zeta_i \Bigg\{ \frac{\omega_{j_n}^2}{\omega_{i_n} \alpha_r^{km}} \Big(A_i(t-t_r)A_j(t-t_r) + A_i(t-t_{r-1})A_j(t-t_{r-1}) \Big) \Phi_1' - \frac{\omega_{j_n}^2}{\omega_{i_d} \alpha_r^{km}} \Big[B_i(t-t_r)A_j(t-t_r) + A_j(t-t_{r-1})B_i(t-t_{r-1}) - \frac{\omega_{i_d}}{\omega_{j_d}} \Big(A_i(t-t_r)B_j(t-t_r) + B_j(t-t_{r-1}) \times A_i(t-t_{r-1}) \Big) \Big] \Phi_7' + \frac{\omega_{i_n} \omega_{j_n}^2}{\omega_{i_d} \omega_{j_d} \alpha_r^{km}} \Big(B_i(t-t_r)B_j(t-t_r) + B_i(t-t_{r-1}) \times B_j(t-t_{r-1}) \Big) \Phi_6' - \frac{\omega_{j_n}^2}{\omega_{i_n} \alpha_r^{km}} A_j(t-t_r)A_i(t-t_{r-1})\Phi_2'(t_r-t_{r-1}) - \frac{\omega_{j_n}^2}{\omega_{i_d} \alpha_r^{km}} \Big(B_i(t-t_{r-1})A_j(t-t_r) - B_j(t-t_r)A_i(t-t_{r-1}) \frac{\omega_{i_d}}{\omega_{j_d}} \Big) \Phi_3'(t_r-t_{r-1}) - \frac{\omega_{j_n}^2 \omega_{i_n}}{\omega_{i_d} \omega_{j_d} \alpha_r^{km}} B_i(t-t_{r-1})B_j(t-t_r)\Phi_8'(t_r-t_{r-1}) + \frac{\omega_{j_n}^2}{\omega_{i_n} \alpha_r^{km}} A_i(t-t_r)A_j(t-t_{r-1})\Phi_4'(t_r-t_{r-1}) + \frac{\omega_{j_n}^2}{\omega_{i_d} \alpha_r^{km}} \Big[B_i(t-t_r)A_j(t-t_{r-1}) - \frac{\omega_{i_d}}{\omega_{j_d}} B_j(t-t_{r-1})A_i(t-t_r) \Big] \Phi_5'(t_r-t_{r-1}) \Bigg\} \quad \text{(E2)}$$

$$- \frac{\omega_{j_n}^2 \omega_{i_n}}{\omega_{i_d} \omega_{j_d} \alpha_r^{km}} B_i(t-t_r) B_j(t-t_{r-1}) \Phi_9'(t_r - t_{r-1}) \Bigg\} \Bigg]$$

where $A_i(t)$ and $B_i(t)$ are given by Equations (D8) and (D9). The values of Φ_1' to Φ_9' are obtained from Equations (C3) to (C11), and

$$\Phi_{10}' = -\frac{\omega_{i_n}}{\alpha_r^{km}} \frac{W_1}{L_1} + \frac{W_2}{L_2} \tag{E3}$$

$$\Phi_{11}' = \frac{\omega_{j_n}^3}{\omega_{i_n}^3} e^{-\zeta_j \omega_{j_n} t} \cdot \frac{1}{E_1} (S_1 \cos \omega_{j_d} t + S_2 \sin \omega_{j_d} t)$$

$$+ e^{-\alpha_r^{km} t} \cdot \frac{1}{E_2} (T_1 \sin \beta_r^{km} t + T_2 \cos \beta_r^{km} t) \tag{E4}$$

$$\Phi_{12}'(t) = e^{-\zeta_i \omega_{i_n} t} \cdot \frac{1}{L_1} (U_1 \cos \omega_{i_d} t - U_2 \sin \omega_{i_d} t)$$

$$+ e^{-\alpha_r^{km} t} \cdot \frac{1}{L_2} (V_1 \sin \beta_r^{km} t + V_2 \cos \beta_r^{km} t) \tag{E5}$$

where

$$S_1 = A_1 \nu_1 + A_2 \nu_2 \tag{E6}$$

$$S_2 = A_2 \nu_1 - A_1 \nu_2 \tag{E7}$$

$$T_1 = B_1 \nu_3 - \frac{\omega_{i_n}}{\alpha_r^{km}} B_2 \nu_4 \tag{E8}$$

$$T_2 = B_1 \nu_4 + \frac{\omega_{i_n}}{\alpha_r^{km}} B_2 \nu_3 \tag{E9}$$

$$U_1 = H_1\eta_1 - H_2\eta_2 \tag{E10}$$

$$U_2 = H_1\eta_2 + H_2\eta_1 \tag{E11}$$

$$V_1 = I_1\nu_3 - \frac{\omega_{i_n}}{\alpha_r^{km}} I_2\nu_4 \tag{E12}$$

$$V_2 = I_1\nu_4 + \frac{\omega_{i_n}}{\alpha_r^{km}} I_2\nu_3 \tag{E13}$$

$$W_1 = H_2\rho_1 + H_1\rho_2 \tag{E14}$$

$$W_2 = I_1\rho_3 - \frac{\omega_{i_n}}{\alpha_r^{km}} I_2\rho_4 \tag{E15}$$

$A_1, A_2, B_1, B_2, H_1, H_2, I_1$ and I_2 are given in Appendix C, and

$$\eta_1 = \frac{\omega_{i_d}}{\omega_{i_n}} (1 - 4\zeta_i^2) \tag{E16}$$

$$\eta_2 = \zeta_i(3 - 4\zeta_i^2) \tag{E17}$$

$$\nu_1 = \frac{\omega_{j_d}}{\omega_{j_n}} (1 - 4\zeta_j^2) \tag{E18}$$

$$\nu_2 = \zeta_j(3 - 4\zeta_j^2) \tag{E19}$$

$$\nu_3 = \frac{\beta_r^{km}}{\alpha_r^{km}} \left(\frac{\beta^{2}{}_r^{km}}{\alpha^{2}{}_r^{km}} - 3 \right) \tag{E20}$$

$$\nu_4 = 3\frac{\beta^2{}_r^{km}}{\alpha^2{}_r^{km}} - 1 \tag{E21}$$

$$\rho_1 = \left(\frac{\omega_{i_d}^2}{\omega_{i_n}^2} - \zeta_i\right)^2 - 4\zeta_i^2\frac{\omega_{i_d}^2}{\omega_{i_n}^2} \tag{E22}$$

$$\rho_2 = 4\zeta_i\frac{\omega_{i_d}}{\omega_{i_n}}\left(\frac{\omega_{i_d}^2}{\omega_{i_n}^2} - \zeta_i^2\right) \tag{E23}$$

$$\rho_3 = \left(\frac{\beta^2{}_r^{km}}{\alpha^2{}_r^{km}} - 1\right)^2 - 4\frac{\beta^2{}_r^{km}}{\alpha^2{}_r^{km}} \tag{E24}$$

$$\rho_4 = 4\frac{\beta_r^{km}}{\alpha_r^{km}}\left(\frac{\beta^2{}_r^{km}}{\alpha^2{}_r^{km}} - 1\right) \tag{E25}$$

NRC, NAE LR-601
National Research Council Canada. National Aeronautical Establishment.

A METHOD FOR THE PREDICTION OF WING RESPONSE TO NON-STATIONARY BUFFET LOADS.
Lee, B.H.K. July 1980. 77 pp. (incl. figures and Appendices).

UNCLASSIFIED

1. Buffeting.
2. Wing loading.

I. Lee, B.H.K.
II. NRC, NAE LR-601

A method for the prediction of the response of a wing to non-stationary buffet loads is presented. The time history of the applied load is segmented into a number of time intervals. In each time segment, the non-stationary load is represented by the product of a deterministic shaping function and a statistically stationary random function. An approximate modelling of the load on the wing is given. The wing is divided into panels or elements, and the load is computed from measured or estimated pressure fluctuations at the centre of each panel. A series representation, with terms of the correlated noise type, is used to curve fit the experimentally determined complex buffet pressure power spectral densities. Using the correlated noise form of power spectral density for the random part of the applied load, analytic expressions are derived for the mean square displacement and acceleration response of the wing. An illustration using data available for the F-4E aircraft is included.

NRC No. 18629

NRC, NAE LR-601
National Research Council Canada. National Aeronautical Establishment.

A METHOD FOR THE PREDICTION OF WING RESPONSE TO NON-STATIONARY BUFFET LOADS.
Lee, B.H.K. July 1980. 77 pp. (incl. figures and Appendices).

UNCLASSIFIED

1. Buffeting.
2. Wing loading.

I. Lee, B.H.K.
II. NRC, NAE LR-601

A method for the prediction of the response of a wing to non-stationary buffet loads is presented. The time history of the applied load is segmented into a number of time intervals. In each time segment, the non-stationary load is represented by the product of a deterministic shaping function and a statistically stationary random function. An approximate modelling of the load on the wing is given. The wing is divided into panels or elements, and the load is computed from measured or estimated pressure fluctuations at the centre of each panel. A series representation, with terms of the correlated noise type, is used to curve fit the experimentally determined complex buffet pressure power spectral densities. Using the correlated noise form of power spectral density for the random part of the applied load, analytic expressions are derived for the mean square displacement and acceleration response of the wing. An illustration using data available for the F-4E aircraft is included.

NRC No. 18629

NRC, NAE LR-601
National Research Council Canada. National Aeronautical Establishment.

A METHOD FOR THE PREDICTION OF WING RESPONSE TO NON-STATIONARY BUFFET LOADS.
Lee, B.H.K. July 1980. 77 pp. (incl. figures and Appendices).

UNCLASSIFIED

1. Buffeting.
2. Wing loading.

I. Lee, B.H.K.
II. NRC, NAE LR-601

A method for the prediction of the response of a wing to non-stationary buffet loads is presented. The time history of the applied load is segmented into a number of time intervals. In each time segment, the non-stationary load is represented by the product of a deterministic shaping function and a statistically stationary random function. An approximate modelling of the load on the wing is given. The wing is divided into panels or elements, and the load is computed from measured or estimated pressure fluctuations at the centre of each panel. A series representation, with terms of the correlated noise type, is used to curve fit the experimentally determined complex buffet pressure power spectral densities. Using the correlated noise form of power spectral density for the random part of the applied load, analytic expressions are derived for the mean square displacement and acceleration response of the wing. An illustration using data available for the F-4E aircraft is included.

NRC No. 18629

NRC, NAE LR-601
National Research Council Canada. National Aeronautical Establishment.

A METHOD FOR THE PREDICTION OF WING RESPONSE TO NON-STATIONARY BUFFET LOADS.
Lee, B.H.K. July 1980. 77 pp. (incl. figures and Appendices).

UNCLASSIFIED

1. Buffeting.
2. Wing loading.

I. Lee, B.H.K.
II. NRC, NAE LR-601

A method for the prediction of the response of a wing to non-stationary buffet loads is presented. The time history of the applied load is segmented into a number of time intervals. In each time segment, the non-stationary load is represented by the product of a deterministic shaping function and a statistically stationary random function. An approximate modelling of the load on the wing is given. The wing is divided into panels or elements, and the load is computed from measured or estimated pressure fluctuations at the centre of each panel. A series representation, with terms of the correlated noise type, is used to curve fit the experimentally determined complex buffet pressure power spectral densities. Using the correlated noise form of power spectral density for the random part of the applied load, analytic expressions are derived for the mean square displacement and acceleration response of the wing. An illustration using data available for the F-4E aircraft is included.

NRC No. 18629